Host-guest inclusion systems of Pt(IV)-bis(benzoato) anticancer candidates and cyclodextrins

Elsevier Editorial System(tm) for Inorganica Chimica Acta
Manuscript Draft

Manuscript Number: ICA-D-15-00110R1

Title: Host-guest inclusion systems of Pt(IV)-bis(benzoato) prodrug candidates and cyclodextrins

Article Type: Regular Paper

Keywords: Platinum(IV) prodrug; Lipophilicity; Cellular accumulation; Antiproliferative activity; Cyclodextrins; Host-guest inclusion systems

Corresponding Author: Prof. Domenico Osella,

Corresponding Author's Institution: Università del Piemonte Orientale

First Author: Mauro Ravera

Order of Authors: Mauro Ravera; Elisabetta Gabano; Sabrina Bianco; Giuseppe Ermondi; Giulia Caron; Maura Vallaro; Giorgio Pelosi; Ilaria Zanellato; Ilaria Bonarrigo; Claudio Cassino; Domenico Osella

Abstract: Two small series of Pt(IV) complexes of general formula cis,cis,trans-[PtA2Cl2L2] (A = 2×NH3 or cyclohexane-1R,2R-diamine, dach; L = aromatic carboxylate of different chain length, i.e. -OCO(CH2)nC6H5, n = 0, 1, and 2) were synthesized and fully characterized (including the X-ray structure of one of them). The antiproliferative activity of the complexes was evaluated on a panel of eight cell lines (including a cisplatin-resistant and a nonmalignant cell line) and their cellular accumulation was determined in HCT 116 human colon cancer cells. In contrast with Pt(IV) complexes bearing aliphatic carboxylates where the antiproliferative potency increases as the number of carbon atoms increases as well, in the bis(benzoato) series a clear structure-activity relationship cannot be drawn, pointing out that the aromatic portion plays a role not simply predictable. In order to increase their water solubility, inclusion reactions with cyclodextrins (CDs) were attempted. Phase-solubility tests demonstrated the ability of b-CD to solubilize the [Pt(NH3)2Cl2L2] series only, offering the best result for the prototype [Pt(NH3)2Cl2(C6H5COO)2]. In the case of [Pt(dach)Cl2L2] series completely insoluble adducts were obtained. Two different ways to prepare the host-guest inclusion systems (i.e. simple solubilization at room temperature of [Pt(NH3)2Cl2(C6H5COO)2] in solution containing excess of b-CD or thermal reaction and subsequent isolation of a solid adduct) were exploited and the resulting products were tested for cytotoxicity against cancer cell lines. The presence of b-CD in solution, increasing the water solubility of [Pt(NH3)2Cl2(C6H5COO)2], does not significantly alter its antitumor activity. The solid inclusion system, albeit very soluble itself, has clearly undergone an extensive aggregation, that resulted detrimental for the Pt cellular accumulation and the overall cytotoxicity.

Graphical Abstract - pictogram (for review)

Click here to download high resolution image

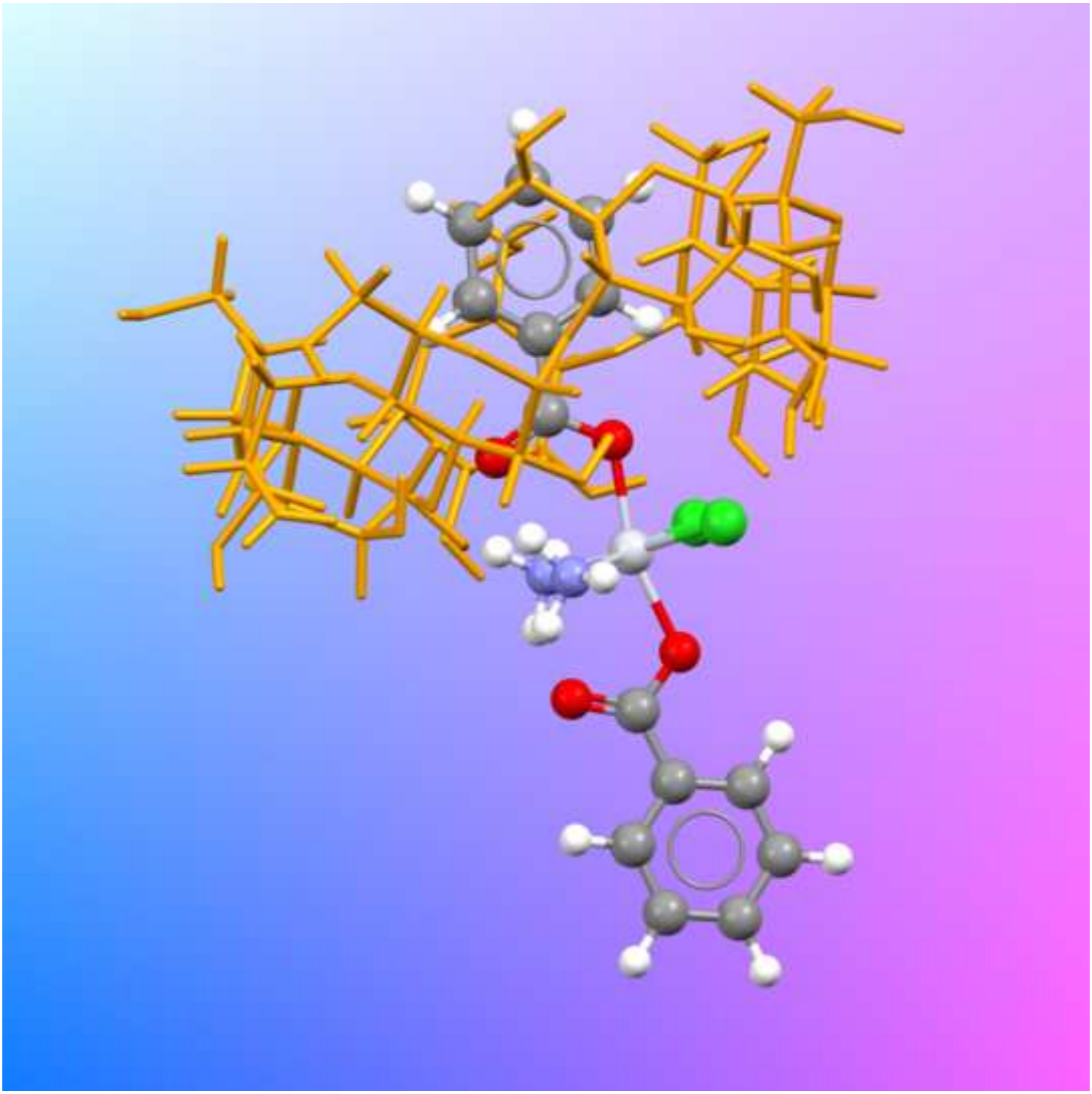

Graphical abstract - synopsis (for review)

Six Pt(IV) *bis*(aromatic carboxylato) anticancer prodrugs based on cisplatin or oxaliplatin were tested for their antiproliferative activity against several cancer cell lines. They resulted very potent, but barely soluble in water. Inclusion systems containing β-cyclodextrin and the prototype $[Pt(NH_3)_2Cl_2(C_6H_5COO)_2]$ have been characterized and tested on the same cell lines.

Highlights

- Biological properties of *bis*(aromatic carboxylato) Pt(IV) complexes are reported
- A clear structure-activity relationship cannot be drawn
- Encapsulation with cyclodextrin (CD) was attempted to increase the water solubility
- Presence of CD in solution does not significantly alter the antitumor activity
- Aggregation in solid adducts is detrimental for cell accumulation and cytotoxicity

Host-guest inclusion systems of Pt(IV)-*bis*(benzoato) anticancer drug candidates and cyclodextrins

Mauro Ravera,[a] Elisabetta Gabano,[a] Sabrina Bianco,[a] Giuseppe Ermondi,[b] Giulia Caron,[b] Maura Vallaro,[b] Giorgio Pelosi,[c] Ilaria Zanellato,[a] Ilaria Bonarrigo,[a] Claudio Cassino,[a] Domenico Osella[a,*]

[a] *Dipartimento di Scienze e Innovazione Tecnologica, Università del Piemonte Orientale, Viale Michel 11, 15121 Alessandria, Italy*

[b] *CASMedChem Research Group at the Centre for Innovation, Dipartimento di Biotecnologie Molecolari e Scienza della Salute, Università di Torino, Via Quarello 11, 10135 Torino, Italy*

[c] *Dipartimento di Chimica, Università di Parma, Parco Area delle Scienze 17A, 43124 Parma, Italy*

[*] Corresponding author. Tel.: +39 0131 360266; fax: +39 0131 360250.
E-mail address: domenico.osella@unipmn.it (D. Osella).

Abstract

Two small series of Pt(IV) complexes of the general formula *cis,cis,trans*-$[PtA_2Cl_2L_2]$ (A = 2×NH_3, series **1**, or cyclohexane-1*R*,2*R*-diamine, dach, series **2**, L = aromatic carboxylate of different chain length, *i.e.* -$OCO(CH_2)_nC_6H_5$, n = 0 (**a**), 1(**b**), and 2(**c**)) were synthesized and fully characterized, including X-ray structure analysis of one of them. The antiproliferative activity of the complexes was evaluated against a panel of eight human cancer cell lines, proving to be at the nanomolar level for the platinum-sensitive A2780 and at the sub-micromolar level for the chemoresistant mesothelioma cell lines. In contrast with Pt(IV) complexes bearing aliphatic carboxylates, whose antiproliferative potency increases with the number of carbon atoms, a clear structure-activity relationship cannot be drawn in the *bis*(benzoato) series. The inclusion reaction with cyclodextrins (CDs), a widely accepted approach for drug formulation, was performed in order to obtain adducts able to bypass the limitations imposed by the low water solubility of *bis*(benzoato) complexes. Phase-solubility tests demonstrated that β-CD was able to efficiently solubilize only the very active prototype $[Pt(NH_3)_2Cl_2(C_6H_5COO)_2]$ **1a**. Two methods were used to prepare the host-guest inclusion systems (*i.e.*, simple solubilization at room temperature of **1a** in solution containing excess of β-CD or thermal reaction with subsequent isolation of a solid adduct) and the resulting adducts were tested for cytotoxicity against the cancer cell lines. The presence of β-CD in solution did not decrease the remarkable antitumor activity of **1a**, whereas the solid-state inclusion system underwent extensive aggregation, proving to be detrimental for Pt accumulation in the cells and, therefore, overall cytotoxicity.

Keywords: Platinum(IV) prodrug, Antiproliferative activity, Lipophilicity, Cellular accumulation, Host-guest inclusion systems, Cyclodextrins.

1. Introduction

In recent years, Pt(IV) complexes have emerged as a possible alternative to traditional Pt(II) anticancer drugs. They are generally considered prodrugs, as they are reduced *in vivo* (in the hypoxic tumor milieu) to the active Pt(II) metabolites after the loss of the two axial ligands (*activation by reduction*) [1]. Pt(IV) complexes exhibit higher chemical inertness than their Pt(II) counterparts and are therefore involved in fewer side (off-target) reactions, thus offering a better tolerability profile and the possibility for oral administration. The equatorial carrier groups are two ammonia molecules (cisplatin-based octahedral scaffold) or the chelating cyclohexane-1*R*,2*R*-diamine, dach (oxaliplatin-like-based octahedral scaffold) depending on the desired cellular selectivity, since the nature of the carrier groups determines the biological activity in the same manner as it does for the Pt(II) complexes [2]. The equatorial leaving groups are generally chlorides or carboxylates, modulating the kinetics of formation of the aquated Pt(II) metabolite. The two axial ligands (very often carboxylates) tune the physicochemical properties, such as lipophilicity and rate of reduction, and greatly influence the overall pharmacokinetic profile.

Pt(IV) complexes bearing aryl carboxylates showed excellent results *in vitro* [3]. In a study on Pt(IV) complexes with aromatic carboxylates containing different functionalities on the ring, Dyson *et al.* found only a moderate correlation among lipophilicity, cellular accumulation and cytotoxic potency. Thus, other than that it confers lipophilicity, the effect of the benzoyl ligands on the activity of the resulting Pt(IV) complexes is not fully understood. Instead, the lipophilicity of Pt(IV) compounds bearing aliphatic carboxylates increases linearly as the number of carbon atoms in the

chain increases, enhancing cellular accumulation and cytotoxicity (at least *in vitro*) [4]. However, there is a limit to such an increase, since the corresponding drop in water solubility limits the bioavailability of the drug. In fact, high lipophilicity corresponds to low water solubility, making the administration of these compounds *in vitro* almost impossible without the (*controversial*) use of organic co-solvents. More importantly for possible clinical use, excessive lipophilicity may result in low intestinal epithelial permeability and, hence, in low oral absorption [5]. Drug performance may be enhanced by using cyclodextrins (CDs) in controlled-release formulations [6], to offset these limitations.

CDs are a family of macrocyclic oligosaccharides, composed of five or more (α-1,4)-linked α-D-glucopyranose units. Typical CDs contain 6 (α-CD), 7 (β-CD), or 8 (γ-CD) monomers (Fig. 1). Due to the chair conformation of the glucopyranose units, CDs are shaped like a truncated cone: all the primary hydroxyl groups are located on one edge of the ring and the secondary ones on another. The cavity of the CDs is made up by skeletal carbons and ethereal oxygens and thus hydrophobic, whereas its exterior is hydrophilic [7]. The cavity can therefore form inclusion complexes with non-polar molecules (or part of them) of appropriate shape and size, thereby improving the water solubility of the guest. CDs and their substituted derivatives are widely used as delivery systems to increase the bioavailability of poorly soluble drugs and to increase their chemical and photochemical stability [8]. Although CDs were discovered over a century ago, only recently have they become available in pure enough form to be used in pharmaceutical applications. To date, about 40 different pharmaceutical formulations containing CDs are on the worldwide market [9].

Fig. 1

In the literature, only a limited number of papers deal with the use of CDs as encapsulatory vehicles for Pt complexes. The efficacy of CDs in enhancing the solubility of cisplatin [10], carboplatin, oxaliplatin and nedaplatin has been demonstrated [11,12,13] and patented [14,15,16].

In the field of Pt(IV) prodrugs, only one report on the formation of a 1:1 inclusion system between β-CD and a complex containing 1-adamantanemethylamine has appeared to date [17]. The resulting host-guest inclusion system proved to be active on human neuroblastoma SK-N-SH cells, although not as active as cisplatin.

The present work studies two small series of Pt(IV) complexes with the "$[PtA_2Cl_2]$" (A = $2\times NH_3$, series **1**, or A = dach, series **2**, Fig. 1) equatorial arrangement and bearing two axial aromatic carboxylates with different lengths of the spacer -$(CH_2)_n$- between phenyl and carboxylic groups (n = 0, 1, and 2). The series were numerically limited to compounds exhibiting acceptable water solubility for meaningful biological tests. The prototypal, highly cytotoxic complexes **1a** and **2a** have been previously reported [3,18]. The interaction between Pt(IV) drug candidates and CDs was assessed with the purpose of increasing their water solubility. The host-guest encapsulation was explored since the protruding phenyl ring of the axial ligands should be well-suited to fit the cavity of CDs [19].

2. Experimental section

2.1. General

$K_2[PtCl_4]$ (Johnson Matthey and Co.) and all other chemicals (Aldrich) were used without further purification. Cisplatin, **3**, and oxaliplatin-like complex **4** were synthesized and purified according to a procedure in the literature [20].

The purity of the compounds was assessed by analytical RP-HPLC (see below), elemental analysis and determination of Pt content. Elemental analyses were carried out with an EA3000 CHN Elemental Analyzer (EuroVector, Milano, Italy). Platinum was quantified by means of a Spectro Genesis ICP-OES spectrometer (Spectro Analytical Instruments, Kleve, Germany) equipped with a crossflow nebulizer. To quantify the platinum concentration, the Pt 299.797 nm line was selected. A platinum standard stock solution of 1000 mg L^{-1} was diluted in 1.0% v/v nitric acid for preparation of calibration standards.

The multinuclear NMR spectra were measured on a Bruker Advance III spectrometer operating at 500 MHz (^{1}H), 125.7 MHz (^{13}C) and 107.2 MHz (^{195}Pt with a spectral window of 2000 ppm), respectively. ^{1}H and ^{13}C NMR chemical shifts were reported in parts per million (ppm) referenced to solvent resonances; for D_2O measurements 1% methanol was added as ^{13}C internal reference. ^{195}Pt NMR spectra were recorded using a solution of K_2PtCl_4 in saturated aqueous KCl as the external reference. The shift for K_2PtCl_4 was adjusted to -1628 ppm from Na_2PtCl_6 ($\delta = 0$ ppm).

RP-HPLC and mass analysis were performed using a Waters HPLC-MS instrument equipped with an Alliance 2695 separation module, a 2487 dual lambda absorbance detector, and a 3100 mass detector. Electrospray ionization mass spectra (ESI-MS) were obtained by delivering a diluted solution of the compound in methanol directly into the spectrometer source at 0.01 mL min^{-1}. The source and desolvation temperatures were

set to 150 and 250 °C, respectively, with nitrogen used both as a drying and a nebulizing gas. The cone and the capillary voltages were usually 30 V and 2.70 kV, respectively. The quasi-molecular ion peaks were assigned on the basis of the *m/z* values and of the simulated isotope distribution patterns.

UV-visible measurements were recorded with a JASCO V550 spectrophotometer.

2.2 Synthesis of platinum complexes

Complexes **1a** [3] and **2a** [18] were prepared according to procedures in the literature. Complexes **1b**, **1c**, **2b**, and **2c** were prepared using slight modifications of the previous methods, starting from the dihydroxido Pt(IV) complexes *cis*,*cis*,*trans*-$[PtCl_2(NH_3)_2(OH)_2]$ and *cis*,*cis*,*trans*-$[PtCl_2(dach)(OH)_2]$ (dach = cyclohexane-1*R*,2*R*-diamine) obtained by oxidation with hydrogen peroxide of **3** and **4**, respectively [4,21].

Briefly, a solution of 2-phenylethanoyl chloride (1.02 mL, 7.8 mmol) or 3-phenylpropanoyl chloride (1.16 mL, 7.8 mmol) in 5 mL of acetone was added dropwise to a suspension of *cis*,*cis*,*trans*-$[PtCl_2(NH_3)_2(OH)_2]$ (100 mg, 0.30 mmol) or *cis*,*cis*,*trans*-$[PtCl_2(dach)(OH)_2]$ (124 mg, 0.30 mmol) in 3 mL of acetone and 1 mL of pyridine. The reaction mixture was stirred at reflux for 4 h. After cooling the solution to RT, excess hexane was added and the resulting precipitate was eliminated by filtration. After removing the solvent under reduced pressure, diethyl ether was added, leading to the precipitation of a white solid. The product was washed with water and dried in *vacuo*.

1b: Yield 77 mg, 0.14 mmol, 45%. ^{1}H-NMR (CD_3OD): δ 3.76 (s, 4H, 2 CH_2), 7.28 (tt, 2H, H_p, ^{3}J = 7.4 Hz, ^{4}J = 1.4 Hz), 7.34 (t, 4H, H_m, ^{3}J = 7.4 Hz), 7.38 (m, 4H, H_o)

ppm. ^{13}C-NMR (CD_3OD): δ 42.1 (CH_2), 126.2 (C_p), 127.9 (C_m), 129.2 (C_o), 135.9 (C_q), 180.7 (C(O)O) ppm. ^{195}Pt-NMR (CD_3OD): δ 1086 ppm. ESI-MS (positive ion mode): 571.4 *m/z* $[M+H]^+$, 593.8 *m/z* $[M+Na]^+$; calcd for $C_{16}H_{21}Cl_2N_2O_4Pt$ 571.33 *m/z* $[M+H]^+$ and for $C_{16}H_{20}Cl_2N_2NaO_4Pt$ 593.31 *m/z* $[M+Na]^+$. ESI-MS (negative ion mode): 569.3 *m/z* $[M-H]^-$; calcd for $C_{16}H_{19}Cl_2N_2O_4Pt$ 569.32 *m/z* $[M-H]^-$. Anal. Calcd for ($C_{16}H_{20}N_2O_4Cl_2Pt$): C 33.70, H 3.53, N 4.91, Pt 34.20; found: C 33.80, H 3.62, N 4.81, Pt, 34.35. RP-HPLC purity (80% MeOH, 20% H_2O): 98.2 %.

1c: Yield 68 mg, 0.11 mmol, 38%. ^{1}H-NMR (CD_3OD): δ 2.64 (t, 4H, CH_2-Ph, ^3J = 7.9 Hz), 2.88 (t, 4H, CH_2-C(O)O, ^3J = 7.9 Hz), 7.16 (m, 2H, H_p), 7.21 (m, 8H, H_o/H_m) ppm. ^{13}C-NMR (CD_3OD): δ 31.6 (CH$_2$-Ph), 37.3 (CH$_2$-C(O)O), 125.6 (C_p), 127.9 (C_m), 128.2 (C_o), 141.9 (C_q), 181.7 (C(O)O) ppm. ^{195}Pt-NMR (CD_3OD): δ 1083 ppm. ESI-MS (positive ion mode): 599.3 *m/z* $[M+H]^+$, 621.3 *m/z* $[M+Na]^+$; calcd for $C_{18}H_{25}Cl_2N_2O_4Pt$ 599.39 *m/z* $[M+H]^+$ and for $C_{18}H_{24}Cl_2N_2NaO_4Pt$ 621.37 *m/z* $[M+Na]^+$. ESI-MS (negative ion mode): 597.1 *m/z* $[M-H]^-$; calcd for $C_{18}H_{23}Cl_2N_2O_4Pt$ 597.37 *m/z* $[M-H]^-$. Anal. Calcd for ($C_{18}H_{24}N_2O_4Cl_2Pt$): C 36.13, H 4.04, N 4.68, Pt 32.60; found: C 36.0, H 3.57, N 4.46, Pt 32.54. RP-HPLC purity (80% MeOH, 20% H_2O): 97.9 %.

2b: Yield 69 mg, 0.11 mmol, 31%. ^{1}H-NMR (dmso-d_6): δ 0.97 (m, 2H, NH_2-CH-CH_2-C$H_{2(ax)}$), 1.22 (m, 2H, NH_2-CH-C$H_{2(ax)}$-CH_2), 1.46 (m, 2H, NH_2-CH-CH_2-C$H_{2(eq)}$), 2.12 (m, 2H, NH_2-CH-C$H_{2(eq)}$-CH_2), 2.44 (m, 2H, NH_2-CH-CH_2-CH_2), 3.60 (s, 4H, 2 CH_2), 7.21-7.30 (m, 10H, H_o, H_m and H_p), 8.18 and 9.37 (m, 4H, NH_2) ppm. ^{13}C-NMR (dmso-d_6): δ 23.4 (c), 31.9 (b), 42.8 (CH$_2$), 62.5 (a), 126.4 (C_p), 128.1 (C_m), 129.2 (C_o), 135.7 (C_q), 180.9 (C(O)O) ppm. ^{195}Pt-NMR (dmso-d_6): δ 1088 ppm. ESI-MS (positive ion mode): 651.3 *m/z* $[M+H]^+$, 673.3 *m/z* $[M+Na]^+$; calcd $C_{22}H_{29}Cl_2N_2O_4Pt$ 650.12 *m/z* $[M+H]^+$ and for $C_{22}H_{28}Cl_2N_2NaO_4Pt$ 672.10 *m/z* $[M+Na]^+$. ESI-MS (negative ion

mode): 649.0 *m/z* [M-H]$^-$; calcd for $C_{22}H_{27}Cl_2N_2O_4Pt$ 648.10 *m/z* [M-H]$^-$. Anal. Calcd for ($C_{22}H_{28}Cl_2N_2O_4Pt$): C 40.62, H 4.34, N 4.31, Pt 29.99; found: C 40.25, H 4.12, N 4.09, Pt 29.64. RP-HPLC purity: 98.8 %.

2c: Yield 67 mg, 0.10 mmol, 30%. ^{1}H-NMR (dmso-d_6): δ 0.99 (m, 2H, NH_2-CH-CH_2-C$H_{2(ax)}$), 1.18 (m, 2H, NH_2-CH-C$H_{2(ax)}$-CH_2), 1.47 (m, 2H, NH_2-CH-CH_2-C$H_{2(eq)}$), 2.11 (m, 2H, NH_2-CH-C$H_{2(eq)}$-CH_2), 2.32 (m, 2H, NH_2-C*H*-CH_2-CH_2), 2.58 (t, 4H, 4 CH_2-Ph, ^{3}J = 7.59), 2.76-2.83 (m, 4H, 4 CH_2-C(O)O), 7.21-7.30 (m, 10H, H_o, H_m and H_p), 8.25 and 9.17 (m, 4H, NH_2) ppm. ^{13}C-NMR (dmso-d_6): δ 23.26 (*c*), 30.05 (*b*, *C*H_2-Ph), 37.4 (*C*H_2-C(O)O), 62.5 (*a*), 125.8 (C_p), 128.2 (C_m, C_o), 140.9 (C_q), 182.2 (*C*(O)O) ppm. ^{195}Pt-NMR (dmso-d_6): δ 1090 ppm. ESI-MS (positive ion mode): 679.3 *m/z* [M+H]$^+$, 701.3 *m/z* [M+Na]$^+$; calcd for $C_{24}H_{33}Cl_2N_2O_4Pt$ 678.15 *m/z* [M+H]$^+$ and for $C_{24}H_{32}Cl_2N_2NaO_4Pt$ 700.13 *m/z* [M+Na]$^+$. ESI-MS (negative ion mode): 677.0 *m/z* [M-H]-; calcd for $C_{24}H_{31}Cl_2N_2O_4Pt$ 677.13 *m/z* [M-H]$^-$. Anal. Calcd for ($C_{24}H_{32}Cl_2N_2O_4Pt$): C 42.48, H 4.75, N 4.13, Pt 28.75; found: C 42.23, H 4.51, N 3.98, Pt 28.25. RP-HPLC purity: 97.8 %.

*2.3 X-ray structure of **1b***

Suitable crystals were grown by slow evaporation of a methanol solution of complex **1b**. A single crystal measuring 0.5×0.2×0.2 mm, was mounted on top of a glass fiber and used for X-ray diffraction data collection on a SMART APEX2 diffractometer [λ(Mo-Ka) = 0.71073 Å]. The crystal proved to be monoclinic, space group $P2_1/a$ and cell parameters of a = 13.098(1), b = 10.1625(8), c = 14.088(1) Å, β = 90.304(1)°, V = 1875.2(2) Å^3. The asymmetric unit is formed by one independent molecule of the

formula $C_{16}H_{20}Cl_2N_2O_4Pt$, M = 570.33 Da, Z = 4, D_c = 2.02 g cm^{-3}, μ = 7.79 mm^{-1}, F(000) = 1096. A semi-empirical absorption correction based on multiple scanned equivalent reflections was applied and gave 0.3582 < T < 0.7464. A total of 23,052 reflections were collected up to a θ range of 26.99° (±16 h, ±12 k, ±17 l), 4084 independent reflections (R_{int} = 0.04). The SAINT software was used for integration of reflection intensity and scaling, and SADABS for absorption correction [22,23]. Structures were solved by direct methods using SIR97 [24] and refined by full-matrix least-squares on all $F2$ using SHELXL97 [25] implemented in the WinGX package [26]. All the non-hydrogen atoms in the molecules were refined anisotropically. The hydrogen atoms were placed in the ideal positions using riding models. Maximum and minimum transmission were 0.7464 and 0.3582 respectively with goodness of fit on F^2 = 1.038. Final R indices [$I > 2\sigma(I)$] were R_1 = 0.023, wR_2 = 0.064 for the 226 parameters refined. The largest difference peak 1.47 and hole -0.54 e Å^{-3} lie in close proximity of Pt. CCDC983761 contains the supplementary crystallographic data for this paper. These data can be obtained free of charge from The Cambridge Crystallographic Data Centre via http://www.ccdc.cam.ac.uk/data_request/cif.

2.4 Lipophilicity

Chromatographic analysis was used to evaluate the capacity factors of the compounds as reported elsewhere [27,28,29]. Briefly, a chromatogram for each complex (0.25 mM) with every different eluant composition (H_2O/CH_3OH, the methanol fraction, φ, ranging from 40 to 80%) was performed on a C18 column (5 µm Phenomenex Gemini® C18 column, 250×3 mm ID). The corresponding retention time t_R

was used to calculate log k' ($k' = (t_R - t_0) / t_0$); KCl was the internal reference to determine the column dead-time, t_0. From these data, extrapolation of the log k' to 0% MeOH (log k'_0), corresponding to the ideal capacity factor in pure water, was performed according to the following formula:

$\log k' = \log k'_0 - S\varphi$

where S is a constant related to solute, solvent, and stationary phase under consideration.

2.5 Reduction with glutathione, α-tocopherol and ascorbic acid

The rate of reduction between Pt(IV) complexes (0.5 mM) and glutathione (5 mM) was evaluated according to the previously reported UV-visible method within 48 h [30,31]. The reduction of Pt(IV) complexes with α-tocopherol ([Pt] = 0.5 mM and [α-tocopherol] = 0.5 mM in 90/10 MeOH/HEPES solution) and with ascorbic acid ([Pt] = 0.25 mM and [ascorbic acid] = 2.5 mM in 70/30 MeOH/HEPES solution) were studied by monitoring the decrease of the area of the Pt(IV) chromatographic peaks in HPLC-MS (see lipophilicity measurements for chromatographic conditions).

*2.6 Water solubility of **1a-2c** and phase-solubility diagrams (Higuchi-Connors method)*

Pt(IV) complexes were weighed into 2-mL Safe-Lock microcentrifuge tubes, then 1 mL of milliQ water was added and the mixture continuously shaken at 25 °C for 24 h. The samples were filtered through a 0.22 μm cellulose nitrate membrane filter, and the Pt content was measured by ICP-OES after proper dilution. According to this procedure,

the solubilities are: **1a** 0.304 ± 0.015, **1b** 0.312 ± 0.003, **1c** 0.121 ± 0.005, **2a** (1.06±0.32)×10^{-2}, **2b** 0.136±0.011, **2c** (5.05±1.80)×10^{-2} mM, respectively.

The phase-solubility diagrams were obtained according to the method reported by Higuchi and Connors [32]. Pt(IV) complexes were weighed into 15-mL Falcon tubes, adding 10 mL of milliQ water containing increasing concentrations of α-CD (0.010-0.100 M range), β-CD (0.002-0.015 M range), and γ-CD (0.002-0.120 M range). In all cases, the maximum [CD] was near its solubility limits. These tubes were sealed and continuously shaken at 25 °C for 24 h. The samples were filtered with a syringe through a 0.22 μm cellulose nitrate membrane filter, and the Pt content was measured by ICP-OES. In the phase-solubility diagram [Pt] is reported *vs.* [CD]; each point is the mean of 3 independent experiments ± standard deviation (SD).

2.7 Determination of the stoichiometry of the CD inclusion complex

The stoichiometry of the inclusion complex of **1a** with β-CD was determined using Job's method, also known as the continuous variation method. In this experiment, seven samples were prepared from two stock solutions with equimolar concentrations of **1a** in methanol and β-CD in ultrapure water, by mixing different volumes of these two solutions and suitable volumes of water and methanol. The resulting samples have the following features: total concentration of host + guest ([**1a**] + [β-CD]) = 1 mM, total volume and methanol/water ratio constant in all samples, and the molar fraction of the guest χ_{1a} (χ_{1a} = [**1a**] / ([**1a**] + [β-CD]) varying in the range 0.2-0.8 ($0.2 < \chi_{\mathbf{1a}} < 0.8$). The variation of an experimental measured property that is sensitive to the inclusion complex formation, in the actual case the maximum UV absorption at 233 nm, A_{sample},

is then monitored in all samples after their dilution to 30 μM with ultrapure water. The maximum in the plot of $(A_{\mathbf{1a}}\text{-}A_{sample})\chi_{\mathbf{1a}}$ (*i.e.* the difference between A_{233} of **1a** and A_{233} of each sample, multiplied by the molar fraction of the guest **1a**) *vs.* the molar fraction of the host β-CD (χ_{CD}) gives the stoichiometry of the inclusion complex (Fig. S3, Supplementary data) [33].

*2.8 Preparation of **1a**-β-CD inclusion systems in solution (**1aHC**) and at the solid state (**1aCD**)*

The **1a**-β-CD adduct in solution was obtained following the above-reported Higuchi-Connors procedure (see section 2.6). Complex **1a** was weighed into 2-mL Safe-Lock microcentrifuge tubes, then 1 mL of milliQ water was added and the mixture continuously shaken at 25 °C for 24 h in the presence of a 15 mM concentration of β-CD. The sample was filtered through a 0.22 μm cellulose nitrate membrane filter; the solution (**1aHC**) contains β-CD and **1a** in 15 mM and 1.13 mM concentration, respectively.

The solid-state adduct **1a**-β-CD was prepared by adding solid β-CD (209 mg, 0.18 mmol) to a suspension of **1a** (50 mg, 0.09 mmol) in 15 mL of water. The reaction mixture was stirred at 70 °C for 24 h to obtain a clear solution. Then, the solvent was removed under reduced pressure, and the product collected as a white solid (**1aCD**).

2.9 Electrochemistry

An Autolab PGSTAT12 electrochemical analyzer (Eco Chemie, Utrecht, The Netherlands) interfaced to a personal computer running GPES 4.9 electrochemical software was used for the electrochemical measurements. A standard three-electrode cell was designed to allow the tip of the reference electrode (saturated calomel electrode, SCE) to closely approach the working electrode (a glassy carbon, GC, disk, diameter 0.1 cm, sealed in epoxy resin). The GC working electrode was polished with alumina followed by diamond paste, then rinsed with distilled water and dried. This process yielded an almost completely reproducible surface for all experiments. All measurements were carried out under nitrogen in 0.1 M $NaClO_4$. The temperature of the solution was kept constant (25±1 °C) by circulation of a thermostated water/ethanol mixture through a jacketed cell. Positive-feedback iR compensation was applied routinely. Four different Higuchi-Connors solutions, containing [β-CD] = 0, 5, 10 and 15 mM, prepared according to section 2.6, were tested.

2.10 Cell culture and growth inhibition (IC_{50})

All the compounds under investigation were tested on three primary MPM cancer cell lines, derived from the pleural effusion of previously untreated patients suffering from MPM, namely BR95 (epithelioid), MM98 (sarcomatoid) [34,35] and MG06 (mixed with epithelioid predominance), and on a cisplatin-resistant cell line called MM98R derived from wild type MM98 by exposure to sub-lethal concentrations of cisplatin for several months [36]. Human mesothelial cells (HMC) were established by gently scraping the peritoneum of the inner wall of uncomplicated congenital hernia sacs surgically excised from premature babies (Pediatric Surgery Unit). This local

environment is usually devoid of significant inflammatory stimuli in the absence of complications and therefore the peritoneum remains thin and almost transparent and the uninjured HMCs are mostly in a normal resting state with a pavement-like appearance. All these cell lines were obtained from the Hospital of Alessandria (Pathology Unit). The human ovarian carcinoma cell line A2780, the human colon carcinoma cell line HCT 116, and the breast cancer cell line MCF-7 were purchased from ECACC (European Collection of Cell Cultures, UK). HMC and epithelioid (BR95 and MG06) cells were grown in Ham's F10 cell medium (GIBCO, Invitrogen Life Science, San Giuliano Milanese, Italy), whereas DMEM (Sigma-Aldrich or Hy-Clone) was used for the sarcomatoid cells. A2780 cells were grown in RPMI1640, and MCF-7 were grown in DMEM supplemented with non-essential amino acids, whereas McCoy's 5A was used for HCT 116 cells. All media were supplemented with L-glutamine (2 mM), penicillin 100 IU mL^{-1}, streptomycin (100 mg L^{-1}) and 10% fetal bovine serum (FBS). Cell culture and treatment were carried out at 37 °C in a 5% CO_2 humidified chamber. Cells were challenged with the compounds under study for 72 h of continuous treatment. Cisplatin, **3**, was dissolved in 0.9% w/v NaCl aqueous solution brought to pH = 3 with HCl (final stock concentration 1 mM). The Pt(IV) complexes (series **1** and **2**) and **4** were dissolved in DMSO (final stock concentration 5 mM) and stored at -66 °C. The inclusion complex **1aCD** was dissolved in ultrapure water (final stock concentration 1 mM), whereas **1aHC** was used directly as the mother solution. The mother solutions were diluted in complete medium, to the required concentration range. In the case of co-solvent, the total DMSO concentration never exceeded 0.2% (this concentration was found to be non-toxic to the cells tested).

To assess the growth inhibition of the compounds under investigation, a cell viability test, *i.e.* the resazurin reduction assay was used [37]. Briefly, cells were seeded in black sterile tissue-culture treated 96-well plates. At the end of treatment, viability was assayed by 100 µg mL^{-1} resazurin (Acros Chemicals, France) in fresh medium for 1 h at 37 °C, and the amount of the reduced product, resorufin, was measured by means of fluorescence (excitation 535 nm, emission 595 nm) with a Tecan Infinite F200Pro plate reader (Tecan Austria). In each experiment, cells were challenged with the drug candidates at different concentrations and the final data were calculated from at least three replicates of the same experiment performed in triplicate. The fluorescence of 8 wells containing medium without cells were used as a blank. Fluorescence data were normalized to 100% cell viability for non-treated cells. Half inhibiting concentration (IC_{50}), defined as the concentration of the drug reducing cell viability by 50%, was obtained from the dose-response sigmoid using Origin Pro (version 8, Microcal Software, Inc., Northampton, MA, USA).

2.11 Cellular accumulation and accumulation ratio

Cancer cells were treated for 4 h with all of the Pt(IV) complexes under investigation, with the Higuchi-Connors solution **1aHC**, and with the solid inclusion complex **1aCD**. The final platinum concentration in the medium was 10 µM in all cases.

To investigate the possible role of the endocytosis process in the uptake of **1aHC**, the effect a series of endocytosis inhibitors was tested.

To inhibit chlatrin-mediated endocytosis, HCT 116 cells were pre-treated 30 min with chlorpromazine (10 μg mL^{-1}) in complete medium [38]. Alternatively, cells were K^+ depleted by a 5 min hypotonic shock (medium + milliQ 1:1), followed by 30 min in K^+-free buffer (NaCl 140 mM, HEPES 20 mM, $CaCl_2$ 1 mM, $MgCl_2$ 1 mM, 1 mg mL^{-1} D-glucose) or in the same buffer supplemented with KCl 10 mM. In addition, a hypertonic treatment was performed for 30 min with 0.45 M sucrose in complete medium [39].

To investigate the role of macropinocytosis, cells were pre-treated 30 min with 5 mM amiloride hydrochloride [40], or 10 μM cytochalasin D [41], and then washed with phosphate buffered saline (PBS).

To investigate the role of caveolae-mediated endocytosis, cells were cholesterol-depleted with a 30 min pre-treatment with methyl-β-cyclodextrin (2.5 mg mL^{-1}) [42], and then washed with PBS.

In all cases except for the controls, the cells were further challenged for 2 h with **1aHC** or **1a,** in fresh serum-free medium.

To take into account the adsorption of Pt(IV) complexes to sterile plasticware, 100 μL of the culture medium was withdrawn immediately after treatment to measure the net extracellular Pt concentration. After treatment, the cells were washed three times in PBS and harvested by trypsinization. An automatic cell counting device (Countess®, Life Technologies) was used to measure the cell number and the mean diameter from every cell count. About 5×10^6 cells were transferred into a glass tube and spun at 1100 rpm for 5 min at room temperature. The supernatant was carefully removed by aspiration, leaving about 200 μL of the supernatant in order to limit the cellular loss. Cellular pellets were stored at -20 °C until mineralization. After thawing, 70% HNO_3

was added and left for 1 h at 60 °C in an ultrasonic bath. Before the measurement, the HNO_3 was diluted to a final 3% concentration. Platinum determination was performed by inductively coupled plasma-mass spectrometry (ICP-MS, Thermo Optek X Series 2). The instrument settings were optimized in order to yield maximum sensitivity for platinum. For quantitative determination, the most abundant isotopes of platinum and indium (used as internal standard) were measured at *m/z* 195 and 115, respectively.

The level of Pt found in cells after the treatment was normalized to the cell number and the cellular volume, calculated from the actual mean cell diameter measured for each sample, in order to obtain the intracellular Pt concentration. The ratio between the intracellular and the known extracellular concentration of Pt is defined as the accumulation ratio, AR [43,44].

2.12 Apoptosis induction

In order to detect caspase 3/7 activity, 20×10^3 A2780 cells were seeded in 96-well tissue culture plates the day before treatment and then challenged with concentrations of drugs approaching 1×, 10×, and 50×IC_{50} values (namely, 0.5. 5 and 25 μM for cisplatin (5, 50, 250 nM for **1a** and **1aHC**). After 24, 48 and 72 h, cells were washed with PBS, and then lysed with 25 μL lysis buffer (10 mM HEPES, 2 mM EDTA, 2 mM dithiothreitol, 0.1% CHAPS, pH 7.4). The caspase 3/7 inhibitor N-Acetyl-Asp-Glu-Val-Asp-CHO (Ac-DEVD-CHO, final concentration 0.01 g L^{-1}) was added to control wells. Then, 200 μL of the caspase-3/7 fluorescent substrate N-Acetyl-Asp-Glu-Val-Asp-7-amido-4-trifluoromethylcoumarin (Ac-DEVD-AFC, 0.01 g L^{-1} in lysis buffer) was added to all wells, mixed, and 200 μL of each sample were transferred to a black

microtiter plate. The activity was observed for 1 h, by means of fluorescence at λ_{exc} = 390 nm and λ_{em} = 520 nm, normalized over the blank [45]. Final activity was computed with respect to the control wells and normalized on the residual viability.

Apoptosis was confirmed by means of annexin V / propidium iodide (PI) staining. Briefly, A2780 cells were treated for 72 h with 50×IC_{50} of Pt complexes (*i.e.*, 25 µM for cisplatin, 250 nM for **1a** or **1aHC**, respectively). After a PBS wash, cells were harvested by trypsinization, counted, and resuspended to a final concentration of 10^6 cell ml^{-1} in 1×annexin V binding buffer (10 mM HEPES/NaOH pH 7.4, 140 mM NaCl, 2.5 mM $CaCl_2$). Cells (400 µL) were incubated 15 min in the dark with 20 µL of stock annexin V-FITC (Life Technologies) and 20 µL of PI stock (10 mg mL^{-1}), then diluted to 2 ml with 1×annexin V binding buffer and immediately analyzed. Flow cytometry analysis was performed using a Partec CyFlow Space (Partec GmbH, Muenster, Germany).

2.13 Molecular modeling

The crystallographic structure of **1a** is available [3] and was used as the starting point for the conformational analysis available in Spartan '10 (Wavefunction Inc., Irvine, CA, USA) with no further modifications. Briefly, the algorithm rotated each single acyclic bond by a specified angle and created a list of conformers that were submitted to a full minimization using PM6 semi-empirical Hamiltonian [46] and the default parameters [28]. Rotation angles were chosen so as to obtain a balance between an accurate exploration of conformational space and CPU time.

The starting conformers of the three CDs were obtained from the Cambridge Structural Database (CSD) [47]. In particular WILJAC, TUXKUS and NUNRIX were

used for α-, β-, and γ-CD, respectively. The structures were used after deletion of ligands and solvent molecules. All the starting structures were submitted to a full minimization run using the same protocol adopted for complex **1a** (see above).

A well-known QM method [48] was used to search for the global minimum of the host-guest inclusion complexes of **1a** with the three CDs. Briefly, the glycosidic oxygen atoms of the CDs were used to define the XY plane and the center of this plane was identified as the center of the coordinates system. Complex **1a** was placed along the Z axis of the coordinates system with the platinum in the center, and then it was allowed to enter and pass through the CD molecule by steps. The guest was moved along the Z-axis from -10 to 10 Å with respect to the initial coordinates. To further improve the accuracy of the approach, the guest molecule was rotated along the Z axis to find the optimal angle at each step. For each step, the complex was rotated by an angle corresponding to 360° divided by the number of glucose units. The geometry of the complex was fully optimized at each step as described above.

The binding energy was evaluated as the difference between the total energy of the **1a**-CD adduct and the total energy of the single host (CD) and guest (**1a**) molecules in two conformations: *i)* the conformation of minimum energy in the adduct (adduct conformation) and *ii)* the free full-minimized conformation, respectively (Table 2). The lower the stabilization energy is, the more thermodynamically favorable is the inclusion complex [49].

2.14 Dynamic Light Scattering (DLS) measurements

Dynamic Light Scattering experiments were carried out on aqueous solutions at 298 K, by using a Zetasizer NanoZS (Malvern, UK) operating in a particle size range from 0.6 nm to 6 μm, and equipped with a He-Ne laser with λ = 633 nm. Before analysis, each sample was diluted with distilled water (final concentration ca. 1 mM).

3. Results and Discussion

*3.1. Synthesis and characterization of complexes **1a-1c** and **2a-2c***

The complexes were prepared according to the reaction scheme shown in Fig. 2. Cisplatin, **3**, and [$PtCl_2$(dach)], **4**, obtained from K_2PtCl_4 using the standard Dhara synthesis [20], were oxidized to the dihydroxido complexes in aqueous solution using 35% hydrogen peroxide. The final carboxylation reaction with benzoyl, 2-phenylethanoyl or 3-phenylpropanoyl chloride was carried out in acetone at 70 °C producing the corresponding *bis*(carboxylato)platinum(IV) complexes **1a**-**1c** and **2a**-**2c** in good yields (Fig. 2).

Fig. 2

The new complexes **1b**, **1c**, **2b** and **2c** were fully characterized by elemental analysis, multinuclear NMR (^{1}H, ^{13}C, and ^{195}Pt), HPLC, and ESI-MS, and in the case of **1b** also by X-ray diffraction. ^{1}H and ^{13}C, NMR signals are consistent with those already reported for **1a** [3] and **2a** [18], apart from additional methylenic signal/s. The ^{195}Pt NMR spectra display a single resonance in the range of 1080-1090 ppm, which is

consistent with a "$Cl_2N_2O_2$" core [3,18,27]. In the parent Pt(II) complexes **3** and **4** ^{195}Pt resonates at -2142 ppm (in D_2O) and -2278 ppm (in DMSO), respectively, more than 3200 ppm upfield relative to the Pt(IV) analogues.

Finally, the identity of the complexes was confirmed using ESI-MS spectra (both measured in positive and negative ion modes). The peak assigned to $[M+H]^+$ (positive ion mode) and $[M-H]^-$ (negative ion mode) usually exhibited the highest relative intensity. The *m/z* values and the isotopic patterns were in agreement with the expected chemical formulas.

*3.2 Crystal structure of complex **1b***

The crystal structure of compound **1b** is shown in Fig. 3. As can be seen in the ORTEP plot, the Pt(IV) coordination geometry is a distorted octahedron. Two Cl atoms and two ammine groups lay *cis* to each other in a square-planar arrangement around the metal atom in a fashion similar to that of **3**, whereas the two remaining *trans* positions are occupied by two carboxylate oxygen atoms belonging to the phenylacetate ligands.

Fig. 3

Both phenylacetate residues behave as monodentate ligands through an oxygen, but the two carboxylate moieties have different orientations with respect to the equatorial coordination plane. The non-coordinated carboxylic oxygen O4 is involved in tight hydrogen bonds with both ammine groups bound to the platinum ion, whereas the analogous O2 oxygen of the other phenylacetate group forms a single hydrogen bond

with only one ammine nitrogen. The other ammine nitrogen is instead involved in an additional hydrogen bond with a chlorine of an adjacent molecule in position -x+1/2+1,+y-1/2,-z and this interaction produces a ribbon of molecules which can be considered the basic pattern of the crystal packing (Fig. S1, Supplementary data).

Similar patterns were also observed in previously reported analogous compounds, where the crystal packing is also mainly determined by hydrogen bonds [3,18].

The novelty in this structure is that, thanks to the presence of the methylene spacer between the carboxyl group and the phenyl ring that prevents delocalization and allows a certain degree of freedom in rotation, interactions between the aromatic rings significantly contribute to determining the packing (Fig. S2, Supplementary data). The phenyl rings of one molecule interact through reciprocal face-to-edge phenyl interactions with a second molecule to form dimeric units. Further weak interconnections can be noticed between dimers through phenyl face-to-face interactions and the combination of these two π-π interaction types provide, along with the N-H···Cl hydrogen bond system cited above, a secondary pattern that characterizes this crystal packing.

3.3 Lipophilicity

Pt(IV) complexes are believed to cross the cellular membrane by passive diffusion alone, since their reactivity towards transport proteins has been found to be negligible [50]. Therefore, their high lipophilicity is expected to enhance cellular uptake, accumulation, and, possibly, cytotoxicity. A stringent correlation between lipophilicity

and the antitumor activity of Pt(IV)-based drugs has been widely described for complexes containing aliphatic carboxylate axial ligands [4].

The lipophilicity of a molecule is usually represented by the logarithmic value of the octanol/water partition coefficient of the compound ($\log P_{o/w}$) determined by the traditional shake-flask method. However, this procedure is not efficient in the case of extremely lipophilic or hydrophilic molecules, and is often surrogated by RP-HPLC measurements [51,52]. In this method, the lipophilicity index is derived from the logarithmic value of the HPLC retention factor ($\log k'$) extrapolated to 100% water ($\log k'_0$, see Experimental section), a parameter closer to $\log P_{o/w}$. Table 1 shows the $\log k'_0$ values measured for the compounds of the two series.

Table 1

The title complexes are by far more lipophilic (higher $\log k'_0$ values) than the corresponding Pt(II) parent compound (**3** and **4**, respectively). However, the differences between **a**-**c** complexes within the same series are small and irregular. In fact, the introduction of one or two methylene groups between the phenyl and the carboxylic group has an unpredictable effect on the final $\log k'_0$ value; in contrast, aliphatic analogues of the general formula *cis*,*cis*,*trans*-[$PtCl_2(NH_3)_2$(carboxylato)$_2$] and *cis*,*cis*,*trans*-[$PtCl_2$(dach)$_2$(carboxylato)$_2$] show a progressive increase of lipophilicity with the number of methylene groups in the axial ligands [4,28].

Nys and Rekker suggested a method for calculating lipophilicity classified as the "additive method", where a molecule is dissected into basic fragments (functional groups or atoms) and its $\log P_{o/w}$ value is obtained by adding the contributions of each

fragment [53]. Interestingly, this approach has been proven valid for Pt(IV) derivatives by Lippard *et al.* [54]. Considering a constant contribution by each "PtA_2Cl_2" moiety to log k'_0 value [55], this procedure reproduces the observed irregular trend: benzoic acid, log $P_{o/w}$ = 1.87, 2-phenylacetic acid log $P_{o/w}$ = 1.41, and 3-phenylpropionic acid log $P_{o/w}$ = 1.84 [56,57].

3.4 Reduction reactions

The ability of **1a**-**1c** and **2a**-**2c** complexes to be "activated by reduction" in the presence of three biologically relevant reducing agents was studied. The three reductants were: *a)* ascorbic acid, AA, *b)* glutathione (γ-glutamylcysteinylglycine), GSH, both present in cytosol, and *c)* α-tocopherol, found primarily in cell membranes. The reaction with GSH was followed by using UV-visible [30,31] and HPLC-MS measurements, whereas the reaction with α-tocopherol was followed by HPLC-MS alone. The results show that none of the complexes are reduced by the two above-mentioned agents within 48 h.

On the other hand, AA proved to be an efficient reductant for such complexes. The kinetic measurements were performed with a 10-fold excess of AA (*i.e.*, 0.25 mM of title complexes and 2.5 mM of AA in a 70/30 MeOH/HEPES solution) by monitoring the decrease of the area of the Pt(IV) chromatographic peaks. These experimental conditions represent the best compromise for solubilizing both Pt(IV) derivatives and AA. The resulting half-life times $t_{1/2}$ (time required to reduce by half the initial chromatographic peak of complex under investigation) are affected by a high degree of uncertainty: 16.5 h for **1a**, 38 h for **1b**, 57 h for **1c**, 12 h for **2a**, 11 h for **2b**, and 16 h for

2c. Interestingly, dach-based series **2** show a somewhat higher reduction rate with respect to the cisplatin-based series **1**. Bulky equatorial ligands, such as dach, can destabilize the encumbered six-coordinated Pt core and allow a faster reduction to the less congested four-coordinated Pt(II) ones [58,59].

The ESI-MS spectra acquired during the reductions show the formation of **3** or **4** from **1** and **2** series respectively, together with their corresponding solvolysis (i.e., monoaquo and diaquo) products. Thus, the reduction is not associated with any ligand rearrangements of the ligands as found in some similar processes [60,61].

3.5 Cell culture and growth inhibition (IC_{50})

Series **1** and **2** were tested on several human cancer cell lines: three primary malignant pleural mesothelioma MPM (an extremely difficult form of cancer to treat), [62] namely BR95 (epithelioid), MG06 (mixed), and MM98 (sarcomatoid) together with its cisplatin-resistant subline MM98R; the nonmalignant human mesothelial cells (HMC), the ovarian carcinoma A2780 and the colon carcinoma HCT 116. The IC_{50} (*i.e.*, the concentration of compound which reduces cell growth by 50%) values were determined by a cell viability assay (*i.e.*, the resazurin assay). In addition, both the resistance factor (RF defined as the ratio between IC_{50} MM98R and IC_{50} MM98) and the selectivity index (SI, defined as the ratio between IC_{50} HMC and the mean of IC_{50} of BR95, MG06, and MM98) were calculated. All the data are reported in Table 1. Parent complexes **3** and **4** were added to the series for comparison.

All of the Pt(IV) complexes are more active than their respective Pt(II) progenitors, namely **3** and **4**, on all the cell lines. In particular, the IC_{50} values for the Pt-sensitive

A2780 cell line are about two orders of magnitude lower for the title complexes than for the corresponding Pt(II) counterparts, and about one order of magnitude lower for the chemoresistant MPM cell lines. As already observed for other Pt complexes, the epithelial-like MPM cell lines BR95 and MG06 proved more resistant than the sarcomatous counterpart (MM98) [62,63]. For the colon HCT 116 cell line, the increase in potency is more pronounced for oxaliplatin-like series **2** than for cisplatin-like series **1**, as expected for the better performance of the dach carrier ligand on this kind of tumor. In general, **2a-2c** result more cytotoxic than **1a-1c** because of the higher lipophilicity of dach with respect to NH_3. The IC_{50} values within each series are instead quite similar.

Finally, as far as the MPM cells are concerned, all of the title compounds show high SI values, suggesting good selectivity against tumor cells with respect to the nonmalignant counterparts and low RF, indicating an ability to overcome cross resistance with cisplatin. In particular, series **2** exhibits a much lower RF than those of series **1** by virtue of the presence of the dach ligand, having higher lipophilicity and, more importantly, generating structurally different Pt(II) metabolites (namely **3** from series **1** and **4** from series **2**) [64].

3.6 Cellular accumulation

The cellular Pt content is a key parameter in understanding the mechanism of action of a Pt-based drug. This cellular accumulation can be better expressed as a pure number, namely the accumulation ratio (AR), *i.e.*, the ratio between the intracellular and the extracellular (in the culture medium) Pt concentration [43]

The cellular accumulation and AR values (Fig. 4) for complexes **1a-1c**, **2a-2c**, **3** and **4** (10 μM) were measured on HCT 116 cells after 4 h of treatment. Cellular accumulation in HCT 116 cells of all Pt(IV) complexes is far higher than that of their Pt(II) precursors; this explains their increase in cytotoxicity and their lower resistance factor. According to Kelland *et al.*, satraplatin (*bis*(acetato)amminedichloridocyclohexylamineplatinum(IV)) and its congeners offer excellent in vitro performance when the resistance phenomenon is mainly due to a reduced influx or increased efflux of the drug [65].

For these Pt(IV)-*bis*(benzoato) complexes, there is neither a simple relationship between lipophilicity and accumulation nor between accumulation and cytotoxicity, as already reported by Dyson *et al.* [3].

Fig. 4

3.7 Solubility studies

It is well accepted that aqueous solubility (typically determined over 24 h) is a critical factor for any drug. The single-point water solubility of **1a**-**2c** was determined from their saturated solutions at 25°C (solubility values < 0.3 mM). Thus, all of the complexes under investigation can be considered almost insoluble according to the United States Pharmacopoeia (USP), British Pharmacopoeia (BP) or European Pharmacopoeia (Ph. Eur.) solubility criteria. Thus, interaction between series **1** and **2** and CDs was attempted for the purpose of increasing their water solubility. The pendant aromatic of the axial ligands should be well-suited to fit the cavity of CDs [66].

The Higuchi-Connors phase-solubility diagrams [32] for **1a** in the presence of α-, β-, and γ-CD, in water at 25 °C are shown in Fig. 5. The solubility of **1a** increases due to the formation of inclusion complexes with CDs. The stability constants *K* were calculated from the slope of the initial linear portion of the phase-solubility diagrams using the equation K = slope / S_0 (1-slope), where S_0 is the solubility of **1a** in water [67]. The *K* values are 64.7, 170, and 18.9 M^{-1}, with α-, β-, and γ-CD, respectively. In all cases, the above-mentioned slope is less than one, indicating the formation of a 1:1 Pt(IV)/CD complex. The stoichiometry of the Pt(IV)/CD complex was confirmed by Job's plot (Fig. S3, Supplementary data) [33], where a maximum at 0.5 indicates the existence of an adduct with a 1:1 molar ratio.

Fig. 5

The shape of solubility plot for **1a** and both α- and β-CD shows an A-type profile that is obtained when the solubility of the guest increases with increasing host concentration. The A_L-solubility curve obtained with β-CD, together with its slope, further indicate that only a 1:1 inclusion complex is formed in solution. Instead, the A_N-type solubility curve obtained for α-CD (where the guest solubility increases linearly with CD concentration but deviate negatively from the straight line at high [CD]), is much more difficult to interpret. The negative deviation from linearity may be associated with changes in adduct solubility or self-association of cyclodextrin molecules. Finally, the B-type curves obtained in the case of γ-CD indicate the formation of inclusion complexes with intrinsically limited solubility in water [6]. Among the three hosts, β-CD shows the highest increase of solubility of **1a** (about 4

times at [β-CD] = 15 mM), whereas α-CD offered worse results because of a lower *K* and γ-CD produced a scarcely soluble inclusion system. For these reasons, the remaining work focused only on the use of β-CD.

For complexes **1b** and **1c**, a different scenario was seen. With β-CD, a B-type phase-solubility diagram is observed, showing that a simple increase in the length of the -$(CH_2)_n$- (n = 1, 2) spacer between phenyl and carboxylic groups in the axial ligands leads to a dramatic decrease in the solubility of the corresponding adducts (Fig. S4, Supplementary data). Surprisingly, the spacer does not offer any advantage for the efficacy of inclusion, possibly due to bending of the chain and the resulting intramolecular hydrogen bonds. The same diagram shown for compound **1c** was observed for all complexes belonging to series **2** (data not shown).

3.8 Preparation of solution adduct **1aHc** *and solid-state adduct* **1aCD** *from* ***1a*** *and β-CD*

The procedure for preparing adducts with CDs in aqueous solution is similar to that adopted in the Higuchi-Connors analysis. Only the promising inclusion adduct between **1a** and β-CD (**1aHC**) was further investigated by means of UV-visible spectroscopy and electrochemical methods. Compound **1a** shows a large band at λ_{max} = 233 nm, but in the presence of β-CD the roto-vibrational profile of the phenyl ring is better resolved and red-shifted (Fig. S5, Supplementary data). The shift may be ascribed to the different polarity of the environment, whereas the profile is related to the interaction between the phenyl rings of **1a** and the cavity of β-CD, resulting in the restriction of the freedom of vibration and rotation of the guest [68]. Electrochemical measurements further

corroborated the formation of the inclusion system. Complex **1a** shows the usual Pt(IV) → Pt(II) irreversible $2e^-$ reduction. The voltammetric responses of three different Higuchi-Connors solutions, containing increasing [β-CD] (Fig. S6, Supplementary data), show a progressive cathodic shift of the peak potential as a consequence of the inclusion system formation. Additional energy is required in order to obtain free **1a** from the adduct, so that the cathodic shift is inversely related to the stability constant and to the [β-CD] concentration. At the same time, the adduct increases the concentration of [**1a**] near the electrode and, hence, the intensity (cathodic current) of the reduction peak.

For preparation of solid-state formulations, the co-precipitation method, the neutralization method, the slurry method, the kneading method, and the grinding method were described, among others [69]. In the present case, simple heating (70 °C) of a 1:2 mixture of **1a** and β-CD for 24 h followed by removal of the solvent under reduced pressure provided quantitatively the solid-state inclusion product **1aCD**.

3.9 NMR characterization

NMR technique provides evidence for the host-guest interaction: the inclusion of a guest molecule in the hydrophobic CD cavity generally causes the shift of the signals of all protons directly involved [70].

In **1aHC** the signals assigned to the ortho (H_o), meta (H_m), and para (H_p) aromatic protons are shifted with respect to those of free **1a** (Fig. 6) but not doubled, suggesting a fast exchange (within the NMR time-scale) between the free and CD-included state of

1a. The differences in chemical shift between **1a** and **1aHC** are quite small, according to the low value of $K_{1:1}$.

The ^{1}H-NMR spectra of β-CD and **1aCD** show that the signals of protons H-3, H-5, and H-6, located inside the β-CD cavity, are also shifted, supporting the formation of the inclusion product (Fig. S7 and Table S1, Supplementary data).

To further investigate the structure of the host-guest inclusion complex, a two-dimensional ^{1}H-NMR ROESY (Rotating frame Overhauser Effect SpectroscopY) experiment was performed to shed light on the dipolar interactions established between guest and host protons situated next to each other. The 2D ROESY spectrum (Fig. 6) shows several intermolecular cross-peaks between H-3, H-5, and H-6 protons of β-CD and H_o and H_m of the phenyl groups of **1a**, demonstrating the inclusion of aromatic ring in the CD cavity. No correlations are observed between any internal proton of β-CD and H_p, indicating that this proton points out from the cavity (Fig. 6).

Fig. 6

3.10 Molecular modeling

Figure 7 shows the lowest energy conformers of the three inclusion complexes of **1a** with α-, β-, and γ-CD, respectively. In all the complexes investigated, the ammine ligands of **1a** form hydrogen bonds with the hydroxyl rims of the CDs.

The platinum center is positioned on the primary hydroxyl rim in the case of α-CD, whereas it is located on the secondary hydroxyl rim for β-CD. In the case of γ-CD the bigger dimensions of the cavity allow **1a** to enter more deeply into the host molecule

and to lodge near the center of CD. A few guest molecules penetrate CDs from the narrower primary hydroxyl rim [71]. The minimum energy structure of the adduct **1a**-β-CD is in agreement with NMR data, since the shortest distances are between the CD inner hydrogens and the ortho and para hydrogens as follows: H_m:H-5 (1.79 Å), H_m:H-6 (2.49 Å), H_o:H-3 (2.23 Å) and H_o:H-5 (2.03 Å). Further, in order to quantify the interaction between **1a** and CDs in the optimized geometries, the binding energy, ΔE, was calculated using the following equation:

$$\Delta E = E_{\text{adduct}} - (E_{\mathbf{1a}} + E_{\text{CD}})$$

where E_{adduct} represents the calculated total energy of the optimized most stable inclusion complex, whereas $E_{\mathbf{1a}}$ and E_{CD} represent those of the free **1a** and CD, respectively (see details in the Experimental section). The results reported in Table 2 indicate that the inclusion process of **1a** is thermodynamically favorable with all CDs, but adduct **1a**-β-CD is the most stable. Moreover, **1a**-β-CD shows a pronounced difference in binding energies ΔE and $\Delta E'$, the latter calculated taking into account the free full-minimized conformations for **1a** and CDs. In particular, the most stable β-CD conformation in the adduct is about 11 kcal mol^{-1} less stable than the free full-minimized conformation. α- and γ-CD show a less pronounced difference between the free and inclusion complex conformations (about 2 and 5 kcal mol^{-1}, respectively) suggesting a better propensity of β-CD to adapt its conformation to maximize the interaction with such a guest.

Fig. 7

Table 2

3.11 Dynamic light scattering (DLS) analysis of **1aHC** *and* **1aCD**

Dynamic light scattering (DLS) analysis of **1aHC** and **1aCD** suggests that the two systems have completely different properties. The **1aHC** adduct tends to form aggregates measuring *ca.* 170 nm, whereas the **1aCD** solution is characterized by the presence of larger aggregates of around 1 μm. It is important to note that all DLS measurements were performed at only one fixed angle (173°), so the estimate may be for extremely large or small particle sizes. In fact, for large aggregates, with size of the order of the incident wavelength, the angular-dependence of the scattered light has to be considered [72]. In addition, the scattering intensity is proportional to the sixth power of the diameter of the particle; consequently, smaller particles at low concentrations are hardly detectable in such measurements, and their presence cannot be completely excluded [73].

Taking into account these limitations, the results show that the thermal treatment employed for synthesizing solid-state **1aCD** causes the formation of large aggregates. It has been reported that in aqueous solutions CDs can self-assemble into nano/microsized aggregates [74]. The formation of aggregates increases with increasing CD concentration and stirring. Moreover, the formation of adducts can influence the self-assembly process [75,76]. Unfortunately, due to the relatively low sensitivity of the method, DLS experiments at the very low concentrations employed in the biological experiments cannot be performed to verify the extent of the aggregation in such conditions.

3.12 Biological evaluation of β-CD interaction systems **1aHC** *and* **1aCD**

Cyclodextrin adducts **1aHC** and **1aCD** were tested on the cell lines used in the previous experiments (see sections 3.5 and 3.6, and Table 1). The effect of β-CD alone was initially measured at the highest concentration reached in the culture medium during the biological tests [77]. Cell viability was unaffected by β-CD up to 0.27 mM, a concentration much higher than that administered with the adducts. The data show that **1aHC** is slightly less active (from ca. 1.7 to 2.7 times) than free **1a**, whereas **1aCD** offers the worst results in term of potency, with the ratio of IC_{50}(**1aCD**) / IC_{50}(**1a**) from 100 to 500, depending on the cell line.

It is worthy of note that in an alternative attempt to improve the aqueous solubility of aryl carboxylato Pt(IV) complexes, Ang *et al.* synthesized several axially unsymmetrical derivatives containing other more polar (hydrophilic) ligands besides the benzoates. All these modifications lowered the potency of the new complexes with respect to **1a** [78].

In order to verify whether the different level of cytotoxicity observed for the various adducts of **1a** is affected by a different cell accumulation of the platinum drug, the AR values were determined on the HCT 116 cell line (Fig. 4). The AR of **1aHC** is similar to that of **1a**, in tune with the observed similar cytotoxic activity. Therefore, the **1aHC** formulation seems not to be significantly detrimental for the excellent performance of **1a**. In contrast, the solid inclusion system **1aCD** show a very low AR, which correlates to its negligible cytotoxicity.

Since CDs and their host-guest adducts may enter cells by endocytosis [79], the Pt accumulation of **1aHC** was compared with that of free **1a** in the presence of a series of

inhibitors of micropinocytosis or chlatrin- and caveolae-mediated endocytosis (see Experimental Section). The results show that there are no significant differences in the accumulation for **1a** with respect to the controls (as expected, since its uptake occurs via passive diffusion only) and also for **1aHC** ($p > 0.05$, two sample t-test. Fig. S8, Supplementary data), thus ruling out a significant role for endocytosis in the accumulation of **1aHC**. The mechanism of cellular uptake of **1aHC** consists of the release of free **1a** from the inclusion system **1aHC** outside the cells, followed by passive diffusion (Fig. 8). This hypothesis is consistent with the low thermodynamic stability ($K_{1:1}$ = 170 M^{-1}) of **1aHC**.

In contrast, the heavy aggregation occurring in **1aCD** hampers this dynamic equilibrium that releases free **1a** from the host-guest system, resulting in very limited accumulation and biological activity.

In principle, cisplatin, **1a** and **1aHC** should have an identical mechanism of action, as they are all DNA-damaging agents. Indeed, the host-guest adduct **1aHC** releases free **1a**, which in turn generates cisplatin after intracellular reduction (Fig. 8). After cisplatin aquation, the subsequent formation of intra- and inter-strand Pt-DNA adducts activates cellular sensors of DNA-damage that eventually trigger the apoptotic cascade. As a matter of fact, cisplatin, **1a** and **1aHC** activated apoptosis (Fig. S9, Supplementary data). In particular, the maximum levels of apoptosis (evaluated by caspase 3/7 activity) were observed after 24 h of treatment with cisplatin and after 72 h of treatment with **1a** or **1aHC**. Annexin V/ propidium iodide assay confirmed the occurrence of apoptosis (Fig. S10, Supplementary data).

Fig. 8

4. Conclusions

Two short series of Pt(IV)-*bis*(benzoato) complexes, namely **1a**-**1c** and **2a**-**2c**, have been synthesized and characterized. There is an impressive improvement in lipophilicity, cellular accumulation and cytotoxic potency on passing from Pt(II) to Pt(IV) congeners. Moreover, the Pt(IV) complexes proved significantly active on chemoresistant MPM cell lines. Given the poor prognosis and dearth of effective treatments for this disease, the therapeutic potential of the title complexes warrants further investigation.

A clear structure-activity relationship cannot be drawn for these Pt(IV)-*bis*(benzoato) complexes in contrast with their aliphatic homologues [4,80]; it is possible that the aromatic ligands interact with cellular components through intricate pathways.

A study of the host-guest encapsulation of the title compounds with CDs *via* the pendant aromatic ring reveals that the solubility of the final adducts is strongly dependent on the type of complex and CD. The interaction significantly increases the water solubility only in the case of **1a** with β-CD. Physicochemical experiments confirm the formation of an inclusion complex in solution, **1aHC**, with a 1:1 stoichiometric ratio (one phenyl ring is located inside the cavity of one CD) and with moderate thermodynamic stability ($K_{1:1}$ = 170 M^{-1}). The pharmacological formulation **1aHC** almost completely maintains the excellent antiproliferative activity of free **1a**, whereas the formation of the solid-state adduct **1aCD** causes complete aggregation resulting in poor cellular accumulation and cytotoxicity.

Uptake measurements in the presence of endocytosis inhibitors suggest that **1aHC** quickly releases free **1a**, which enters cells by passive diffusion only (Fig. 8). Finally, as expected, **1a**, **1aHC** and their metabolite cisplatin trigger apoptosis in the treated tumor cells, the most desirable way of eliminating them (Fig. 8).

It is worth mentioning that a very elegant approach to the administration of **1a** has been recently reported by Ang *et al.* [81]. Multi-walled carbon nanotubes entrapped **1a** as a protective shell via hydrophobic interactions, and upon chemical reduction of **1a**, cisplatin is released. At the moment, however, there are many concerns about the possible hazards of such nanoparticles [82], whereas pharmaceutical formulations with CDs are accepted worldwide [9].

5. Abbreviations

AR	accumulation ratio
CD	cyclodextrin
dach	cyclohexane-1*R*,2*R*-diamine
DLS	dynamic light scattering
DMEM	Dulbecco's modified Eagle's medium
DMSO	dimethyl sulfoxide
ESI-MS	electrospray ionization mass spectrometry
FBS	fetal bovine serum
GC	glassy carbon
HEPES	4-(2-hydroxyethyl)-1-piperazineethanesulfonic acid
HPLC-MS	high-performance liquid chromatography-mass spectrometry
IC_{50}	half inhibiting concentration

ICP-MS	inductively coupled plasma-mass spectrometry
ICP-OES	inductively coupled plasma-optical emission spectroscopy
K	stability constant
k'	HPLC retention factor
MPM	malignant pleural mesothelioma
NMR	nuclear magnetic resonance spectroscopy
PBS	phosphate buffered saline
$P_{o/w}$	octanol-water partition coefficient
QM	quantum mechanics
RF	resistance factor
ROESY	rotating frame Overhauser effect spectroscopy
RP-HPLC	reverse-phase high-performance liquid chromatography
RPMI1640	Roswell Park Memorial Institute medium
SI	selectivity index
t_0	column dead-time
t_R	retention time
UV-visible	ultraviolet-visible spectroscopy

Acknowledgments

We thank the CRAL (Alessandria) and CRT (Torino) Foundations for financial support within the joint project "Approcci chemioterapici innovativi per il mesotelioma maligno della pleura". We are indebted to the Inter-University Consortium for Research on the Chemistry of Metals in Biological Systems (CIRCMSB, Bari), and COST

CM1105 Action “Functional metal complexes that bind to biomolecules”, for providing stimulating opportunities for discussion and short-term missions of young researchers. Finally, we thank Drs. Fabio Carniato and Nadia Massa (University of Piemonte Orientale) for DLS and flow cytometric analyses, respectively.

Appendix A. Supplementary data

Crystallographic data (CIF format), hydrogen bonding network and phenyl-phenyl interactions of compound **1b** (Figs. S1 and S2); Job’s plot, UV-visible spectra, voltammetric responses, and ^{1}H-NMR spectra and chemical shifts of **1a** in the presence of β-CD (Figs. S3, S5-S7); phase-solubility diagrams for **1a**-**1c** in the presence of β-CD (Fig. S4); Pt accumulation measured in the presence of different endocytosis inhibitors (Fig. S8); apoptosis induction by the compounds under investigation (Figs. S9 and S10).

References

[1] M.D. Hall, H.R. Mellor, R. Callaghan, T.W. Hambley, J. Med. Chem. 50 (2007) 3403–3411.

[2] T. Fojo, N. Farrell, W. Ortuzar, H. Tanimura, J. Weinstein, T.G. Myers, Crit. Rev. Oncol. Hematol. 53 (2005) 25–34.

[3] W.H. Ang, S. Pilet, R. Scopelliti, F. Bussy, L. Juillerat-Jeanneret, P.J. Dyson, J. Med. Chem. 48 (2005) 8060–8069.

[4] P. Gramatica, E. Papa, M. Luini, E. Monti, M.B. Gariboldi, M. Ravera, E. Gabano, L. Gaviglio, D. Osella, J. Biol. Inorg. Chem. 15 (2010) 1157–1169.

[5] S. Mazzaferro, K. Bouchemal, G. Ponchel, Drug Discovery Today 18 (2013) 25–34.

[6] T. Loftsson, P. Jarho, M. Másson, T. Järvinen, Expert Opin. Drug Deliv. 2 (2005) 335–351.

[7] H. Dodziuk, in: H. Dodziuk (Ed.), Cyclodextrins and Their Complexes, Wiley–VCH, Weinheim, 2006, pp. 1–30.

[8] A. Ahuja, S. Baboota, J. Ali, G. Mustafa, in: E. Bilensoy (Ed.), Cyclodextrins in Pharmaceutics, Cosmetics, and Biomedicine: Current and Future Industrial Applications, John Wiley & Sons, Inc., Hoboken, New Jersey, 2011, pp. 19–43.

[9] T. Loftsson, D. Duchene, Int. J. Pharm. (Amsterdam, Neth.) 329 (2007) 1–11.

[10] A. Balaji, V.P. Pandey, M.S. Srinath, R. Manavalan, Pharmacologyonline, 1 (2009) 1135–1143.

[11] D.R. Alston, T.H. Lilley, J.F. Stoddart, J. Chem. Soc., Chem. Commun. (1985) 1600–1601.

[12] D.R. Alston, A.M.Z. Slawin, J.F. Stoddart, D.J. Williams, J. Chem. Soc., Chem. Commun. (1985) 1602–1604

[13] C.P.A. Anconi, L.d.S. Delgado, J.B. Alves dos Reis, W.B. De Almeida, L.A.S. Costa, H.F. Dos Santos, Chem. Phys. Lett. 515 (2011) 127–131.

[14] Patent: US2011027390–A1

[15] Patent: US4696918

[16] Patent: WO2005102312

[17] Y. Shi, J.C. Dabrowiak, Inorg. Chim. Acta 393 (2012) 337–339.

[18] V. Gandin, C. Marzano, G. Pelosi, M. Ravera, E. Gabano, D. Osella, ChemMedChem 9 (2014) 1299–1305.

[19] K. Harata, in: H. Dodziuk (Ed.), Cyclodextrins and Their Complexes, Wiley–VCH, Weinheim, 2006, pp. 147–198.

[20] S.C. Dhara, Indian J. Chem. 8 (1970) 193–194.

[21] C.M. Giandomenico, M.J. Abrams, B.A. Murrer, J.F. Vollano, M.I. Rheinheimer, S.B. Wyer, G.E. Bossard, J.D. Higgins III, Inorg. Chem. 34 (1995) 1015–1021

[22] SAINT: SAX, Area Detector Integration, Siemens Analytical Instruments Inc., Madison, Wisconsin, USA.

[23] G. Sheldrick, SADABS: Siemens Area Detector Absorption Correction Software, University of Goettingen, Germany, 1996.

[24] A. Altomare, C. Burla, M. Camalli, G. L. Cascarano, C. Giacovazzo, A. Guagliardi, A. G. G. Moliterni, G. Polidori, R. Spagna, J. Appl. Crystallogr., 32 (1999) 115–119.

[25] G.M. Sheldrick, Acta Cryst., 2008, A64, 112–122.

[26] L.J. Farrugia, J. Appl. Crystallogr., 1999, 32, 837–838.

[27] G. Ermondi, G. Caron, M. Ravera, E. Gabano, S. Bianco, J.A. Platts, D. Osella, Dalton Trans. 42(2013) 3482–3489.

[28] J.A. Platts, G. Ermondi, G. Caron, M. Ravera, E. Gabano, L. Gaviglio, G. Pelosi, D. Osella, J. Biol. Inorg. Chem. 16 (2011) 361–372.

[29] J.A. Platts, S.P. Oldfield, M.M. Reif, A. Palmucci, E. Gabano, D. Osella, J. Inorg. Biochem. 100 (2006) 1199–1207.

[30] H. Kostrhunova, J. Kasparkova, D. Gibson, V. Brabec, Mol. Pharmaceutics 7 (2010) 2093–2102.

[31] J.C. Dabrowiak, J. Goodisman, A.-K. Souid, Drug Metab. Dispos. 30 (2002) 1378–1384.

[32] T. Higuchi, K.A. Connors, in: C.N. Reilly (Ed.) Advances in Analytical Chemistry Instrumentation, Vol. 4, Interscience, New York, NY, 1965, pp. 117–212.

[33] C. Tablet, I. Matei, M. Hillebrand, in: A. Innocenti (Ed.) Stoichiometry, Research - The Importance of Quantity in Biomedicine, InTech, Rijeka, Croatia, 2012, ch. 3.

[34] E. Aldieri, C. Riganti, F. Silvagno, S. Orecchia, P. G. Betta, S. Doublier, E. Gazzano, M. Polimeni, A. Bosia, D. Ghigo, Am. J. Respir. Cell Mol. Biol. 45 (2011) 625–631.

[35] S. Orecchia, F. Schillaci, M. Salvio, R. Libener, P.G. Betta, Lung Cancer 45 Suppl. 1 (2004) S37–S43.

[36] I. Zanellato, C.D. Boidi, G. Lingua, P.G. Betta, S. Orecchia, E. Monti, D. Osella, Cancer Chemother. Pharmacol. 67 (2011) 265–273.

[37] E. Magnani, E. Bettini, Brain Res. Protoc. 5 (2000) 266–272.

[38] A.I. Ivanov, Methods Mol. Biol. 440 (2008) 15–33.

[39] S.H. Hansen, K. Sandvig, B. van Deurs, J. Cell Biol. 121 (1993) 61–72.

[40] B.G. Blair, C.A. Larson, P.L. Adams, P.B. Abada, C.E. Pesce, R. Safaei, S.B. Howell, Mol. Pharmacol. 79 (2011) 157–166.

[41] A.K. Holzer, S.B. Howell, Cancer Res. 66 (2006) 10944–10952.

[42] F. Mollinedo, J. de la Iglesia-Vicente, C. Gajate, A. Estella-Hermoso de Mendoza, J.A. Villa-Pulgarin, M. de Frias, G. Roué, J. Gil, D. Colomer, M.A. Campanero, M.J. Blanco-Prieto, Clin. Cancer Res. 16 (2010) 2046–2054.

[43] A. Ghezzi, M. Aceto, C. Cassino, E. Gabano, D. Osella, J. Inorg. Biochem. 98 (2004) 73–78.

[44] E. Gabano, D. Colangelo, A.R. Ghezzi, D. Osella, J. Inorg. Biochem. 102 (2008), 629–635.

[45] K. Kuželová, D. Grebeňová, B. Brodská, J. Cell Biochem. 112 (2011) 3334–3342.

[46] J.J.P. Stewart, J. Mol. Model. 13 (2007) 1173–1213.

[47] F.H. Allen, Acta Crystallogr., Sect. B: Struct. Crystallogr. Cryst. Chem. 58 (2002) 380–388.

[48] L. Liu, Q. X. Guo, J. Inclusion Phenom. Macrocyclic Chem. 50 (2004) 95–103.

[49] A. Fifere, N. Marangoci, S. Maier, A. Coroaba, D. Maftei, M. Pinteala, Beilstein J. Org. Chem. 8 (2012) 2191–2201.

[50] F. Arnesano, S. Scintilla, G. Natile, Angew. Chem. Int. Ed. 46 (2007) 9062–9064.

[51] W.J. Lambert, J. Chromatogr. A 656 (1993) 469–484.

[52] S. Martel, D. Guillarme, Y. Henchoz, A. Galland, J.L. Veuthey, S. Rudaz, P.A. Carrupt, in: R. Mannhold (Ed.) Molecular Drug Properties Measurement and Prediction (Methods and Principles in Medicinal Chemistry, Vol. 37), Wiley–VCH, Weinheim, 2008, ch. 13.

[53] M.S. Tute, in: V. Pliška, B. Testa, H. van de Waterbeemd (Eds.) Lipophilicity in Drug Action, Toxicology (Methods and Principles in Medicinal Chemistry, Vol. 4), VCH, Weinheim, 1996, pp. 7–26.

[54] T.C. Johnstone, S.J. Lippard, Inorg. Chem. 52 (2013) 9915–9920.

[55] G. Caron, G. Ermondi, M.B. Gariboldi, E. Monti, E. Gabano, M. Ravera, D. Osella, ChemMedChem 4 (2009), 1677–1685.

[56] T. Fujita, J. Iwasa, C. Hansch, J. Am. Chem. Soc. 86 (1964) 5175–5180.

[57] J. Iwasa, T. Fujita, C. Hansch, J. Med. Chem. 8 (1965) 150–153.

[58] S. Jovanović, B. Petrović, Ž.D. Bugarčić, R. van Eldik, Dalton Trans. 42 (2013) 8890–8896.

[59] S. Choi, C. Filotto, M. Bisanzo, S. Delaney, D. Lagasee, J.L. Whitworth, A. Jusko, C. Li, N.A. Wood, J. Willingham, A. Schwenker, K. Spaulding, Inorg. Chem. 37 (1998) 2500–2504.

[60] M. Ravera, E. Gabano, I. Zanellato, I. Bonarrigo, E. Escribano, V. Moreno, M. Font–Bardia, T. Calvet, D. Osella, Dalton Trans. 41 (2012) 3313–3320.

[61] A. Nemirovski, I. Vinograd, K. Takrouri, A. Mijovilovich, A. Rompel, D. Gibson, Chem. Commun. 46 (2010) 1842–1844.

[62] I. Zanellato, I. Bonarrigo, E. Gabano, M. Ravera, N. Margiotta, P.G. Betta, D. Osella, Inorg. Chim. Acta 393 (2012) 64–74.

[63] A.A. Mujoomdar, T.R. Tilleman, W.G. Richards, R. Bueno, D.J. Sugarbaker, J. Thorac. Cardiovasc. Surg. 78 (2010) 617–622.

[64] C.A. Rabik, M.E. Dolan, Cancer Treat. Rev. 33 (2007) 9–23.

[65] S.Y. Sharp, P.M. Rogers, L.R. Kelland, Clin. Cancer Res. 1 (1995) 981–989.

[66] K. Harata, in: H. Dodziuk (Ed.), Cyclodextrins and Their Complexes, Wiley–VCH, Weinheim, 2006, pp. 147–198.

[67] S.V. Kurkov, E.V. Ukhatskaya, T. Loftsson, J. Inclusion Phenom. Macrocyclic Chem. 69 (2011) 297–301.

[68] I.M. Trofymchuk, L.A. Belyakova, A.G. Grebenyuk, J. Inclusion Phenom. Macrocyclic Chem. 69 (2011) 371–375.

[69] A.R. Hedges, Chem. Rev. 98 (1998) 2035–2044.

[70] T. Bojinova, Y. Coppel, N. Lauth-de Viguerie, A. Milius, I. Rico-Lattes, A. Lattes, Langmuir 19 (2003) 5233–5239.

[71] S. Siva, J. Thulasidhasan, N. Rajendiran, Spectrochim. Acta, Part A 115 (2013) 559–567.

[72] C. Graf, Q. Gao, I. Schutz, C.N. Noufele, W.T. Ruan, U. Posselt, E. Korotianskiy, D. Nordmeyer, F. Rancan, S. Hadam, A. Vogt, J. Lademann, V. Haucke, E. Ruhl, Langmuir 28 (2012) 7598–7613.

[73] F. Rancan, Q. Gao, C. Graf, S. Troppens, S. Hadam, S. Hackbarth, C. Kembuan, U. Blume–Peytavi, E. Ruehl, J. Lademann, A. Vogt, ACS Nano 6 (2012) 6829–6842.

[74] M. Messner, S.V. Kurkov, P. Jansook, T. Loftsson, Int. J. Pharm. (Amsterdam, Neth.) 387 (2010) 199–208.

[75] M. Messner, S.V. Kurkov, M.M. Palazon, B.A. Fernandez, M.E. Brewster, T. Loftsson, Int. J. Pharm. (Amsterdam, Neth.) 419 (2011) 322–328.

[76] G. Gonzalez–Gaitano, P. Rodriguez, J.R. Isasi, M. Fuentes, G. Tardajos, M.Sanchez, J. Inclusion Phenom. Macrocyclic Chem. 44 (2002) 101–105.

[77] T. Kiss, F. Fenyvesi, I. Bácskay, J. Váradi, É. Fenyvesi, R. Iványi, L. Szente, Á. Tósaki, M. Vecsernyés, Eur. J. Pharm. Sci. 40 (2010) 376–380.

[78] C.F. Chin, Q. Tian, M.I. Setyawati, W. Fang, E.S.Q. Tan, D.T. Leong, W.H. Ang, J. Med. Chem. 55 (2012) 7571–7582.

[79] A.P. Plazzo, C.T. Höfer, L. Jicsinszky, É. Fenyvesi, L. Szente, J. Schiller, A. Herrmann, P Müller, Chem. Phys. Lipids 165 (2012) 505–511.

[80] H.P. Varbanov, M.A. Jakupec, A. Roller, F. Jensen, M. Galanski, B.K. Keppler, J. Med. Chem. 56 (2013) 330–344.

[81] J. Li, S.Q. Yap, C.F. Chin, Q. Tian, S.L. Yoong, G. Pastorin, W.H. Ang, Chem. Sci. 3 (2012) 2083–2087.

[82] W.H. De Jong, P.J.A. Borm, Int. J. Nanomed. 3 (2008) 133–149.

Tables

Table 1. Logarithmic value of the RP-HPLC retention factors extrapolated to 100% water (log k'_0) and IC_{50} (μM) values after 72 h. Data are means ± standard deviation of at least three independent replicates

Compound	log k'_0	IC_{50} [μM]						
		A2780	HCT 116	BR95	MG06	MM98	MM98R	HMC
3	-0.567	0.5 ± 0.1	2.3 ± 0.3	6.2 ± 0.9	4.1 ± 1.5	3.2 ± 1.0	19.4 ± 2.8 [6.1]	6.7 ± 1.2 (1.5)
1a	2.26	$4.0 \pm 0.1 \times 10^{-3}$	$54.0 \pm 10.0 \times 10^{-3}$	0.33 ± 0.09	0.48 ± 0.09	0.12 ± 0.03	0.47 ± 0.08 [3.9]	0.32 ± 0.05 (1.0)
1b	2.34	$49.6 \pm 3.6 \times 10^{-3}$	0.21 ± 0.05	1.97 ± 0.64	1.24 ± 0.57	0.64 ± 0.28	1.23 ± 0.33 [1.9]	4.16 ± 0.80 (3.2)
1c	3.30	$5.4 \pm 0.1 \times 10^{-3}$	$51.0 \pm 5.2 \times 10^{-3}$	0.53 ± 0.27	0.71 ± 0.15	0.20 ± 0.07	0.44 ± 0.12 [2.2]	0.90 ± 0.42 (1.9)
4	-0.131[a]	0.12 ± 0.04	0.27 ± 0.03	1.0 ± 0.2	0.8 ± 0.2	2.2 ± 0.4	2.5 ± 0.6 [1.1]	0.8 ± 0.1 (0.6)
2a	3.02	$2.2 \pm 0.3 \times 10^{-3}$	$2.4 \pm 0.7 \times 10^{-3}$	$21.7 \pm 4.9 \times 10^{-3}$	$38.0 \pm 20.8 \times 10^{-3}$	$15.0 \pm 3.3 \times 10^{-3}$	$18.0 \pm 3.5 \times 10^{-3}$ [1.2]	0.13 ± 0.08 (5.2)
2b	2.55	$1.3 \pm 0.1 \times 10^{-3}$	$2.7 \pm 0.6 \times 10^{-3}$	$14.0 \pm 7.1 \times 10^{-3}$	$82.0 \pm 21.2 \times 10^{-3}$	$62.2 \pm 17.9 \times 10^{-3}$	$71.6 \pm 37.2 \times 10^{-3}$ [1.2]	0.15 ± 0.08 (2.8)
2c	3.68	$3.6 \pm 0.9 \times 10^{-3}$	$4.9 \pm 1.1 \times 10^{-3}$	$19.3 \pm 5.5 \times 10^{-3}$	$90.4 \pm 8.0 \times 10^{-3}$	$58.1 \pm 19.1 \times 10^{-3}$	$32.9 \pm 9.7 \times 10^{-3}$ [0.6]	0.23 ± 0.07 (4.1)
1aHC	-	$7.0 \pm 3.0 \times 10^{-3}$	0.14 ± 0.01	1.3 ± 0.1	0.86 ± 0.01	0.31 ± 0.05	0.89 ± 0.03 [2.9]	0.77 ± 0.03 (0.94)
1aCD	-	1.41 ± 0.03	20.8 ± 3.5	53.2 ± 4.5	55.0 ± 21.2	60.6 ± 8.0	63.7 ± 29.9 [1.1]	42.1 ± 16.5 (0.75)

[a] From ref. [29]. Data in brackets: Resistance factor, RF = (IC_{50} MM98R) / (IC_{50} MM98). Data in parenthesis: Selectivity Index, SI = the ratio between IC_{50} (HMC) and the average IC_{50} on BR95, MG06 and MM98.

Table 2. Calculated total energy *E* of molecules (inclusion systems, **1a** and CDs) and binding energy, ΔE [kcal mol^{-1}]

	Adduct conformation				**Free full-minimized conformation**		
	E_{adduct}	E_1	E_{CD}	**Binding Energy**[a] ΔE	E_1'	E_{CD}'	**Binding Energy**[b] $\Delta E'$
α-CD	-1550.38	-174.69	-1350.37	-25.32	-174.69	-1352.59	-23.10
β-CD	-1771.28	-171.87	-1556.41	-43.00	-174.64	-1567.88	-28.76
γ-CD	-1970.57	-174.55	-1772.67	-23.35	-174.55	-1777.13	-18.90

[a] $\Delta E = E_{adduct} - (E_1 + E_{CD})$; [b] $\Delta E' = E_{adduct} - (E_1' + E_{CD}')$

Captions to Figures

Fig. 1. Sketch of the Pt(IV) complexes under investigation (**1a**-**1c** and **2a**-**2c**) and their corresponding Pt(II) parent compounds (**3** and **4**), along with molecular structures of the cyclodextrins (CDs) under investigation. The CD numbering scheme is reported.

Fig. 2. Synthetic route to prepare complexes **1a**-**1c** (A = NH_3) and **2a**-**2c** (A = dach): *a)* H_2O_2 35%, water, RT, 24 h; *b)* aryl chloride, acetone, reflux 4 h.

Fig. 3. ORTEP plot of compound **1b** with ellipsoids at 50% probability.

Fig. 4. Pt accumulation ratio (AR, see experimental section) in HCT 116 cells of the compounds under investigations and inclusion systems **1aHC** and **1aCD** (all 10 μM, 4 h of treatment). Data are means ± standard deviations of at least 3 independent replicates and were compared by means of the two sample t-test (* $p < 0.5$;** $p < 0.01$; *** $p < 0.001$; n.s. = statistically not significant).

Fig. 5. Phase-solubility diagrams for **1a** in the presence of α- (circles), β- (squares), and γ-CD (triangles) in water solution at 25 °C.

Fig. 6. Expanded region of the ROESY spectrum of **1aCD** and proposed geometry for the inclusion of **1a** into β-CD.

Fig. 7. Minimum energy conformation of the complex between **1a** and (A) α-, (B) β- and (C) γ-CD. CD molecules are oriented with the primary hydroxyl rims in the upper part of the figure whereas the secondary hydroxyl rims are in the lower part of the figure. The models have been obtained by means of molecular modeling calculations.

Fig 8. Sketch of mechanism of action of **1aHC** and its metabolites **1a** and cisplatin (the two electrons come from cellular reductants).

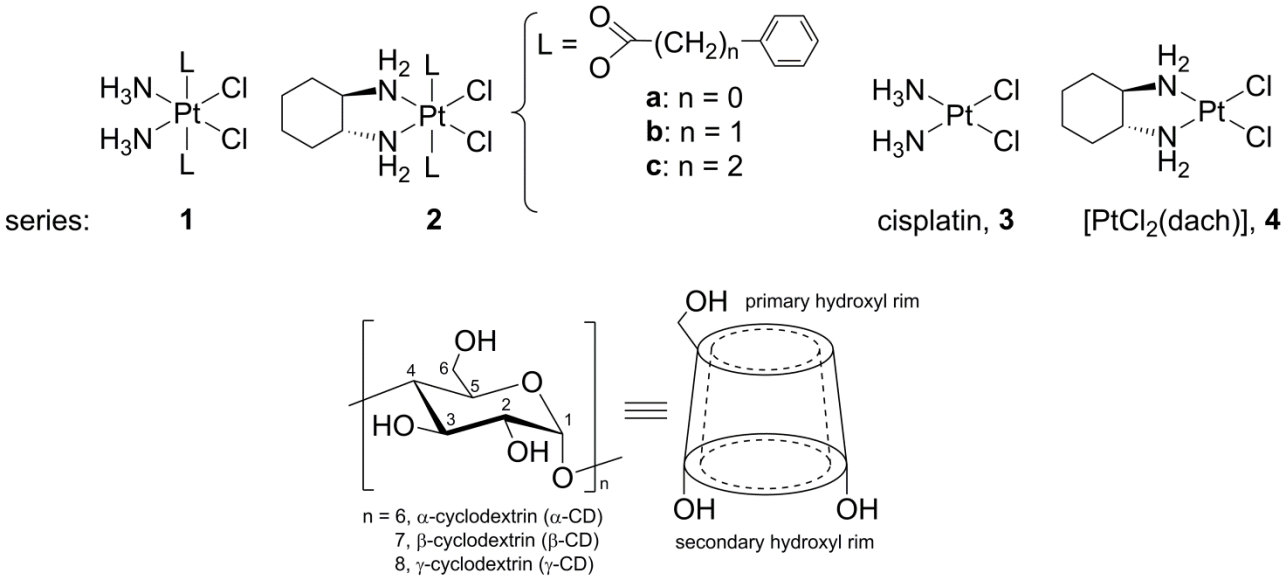
L =
a: n = 0
b: n = 1
c: n = 2
series:
1
2
cisplatin, 3
[PtCl2(dach)], 4
primary hydroxyl rim
secondary hydroxyl rim
n = 6, α-cyclodextrin (α-CD)
7, β-cyclodextrin (β-CD)
8, γ-cyclodextrin (γ-CD)

Fig. 1.

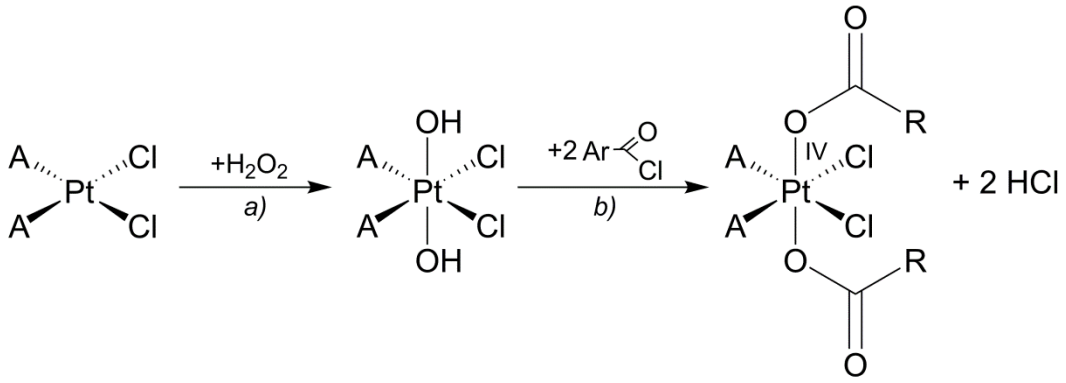
+H2O2
a)
+2 Ar
b)
+ 2 HCl

Fig. 2.

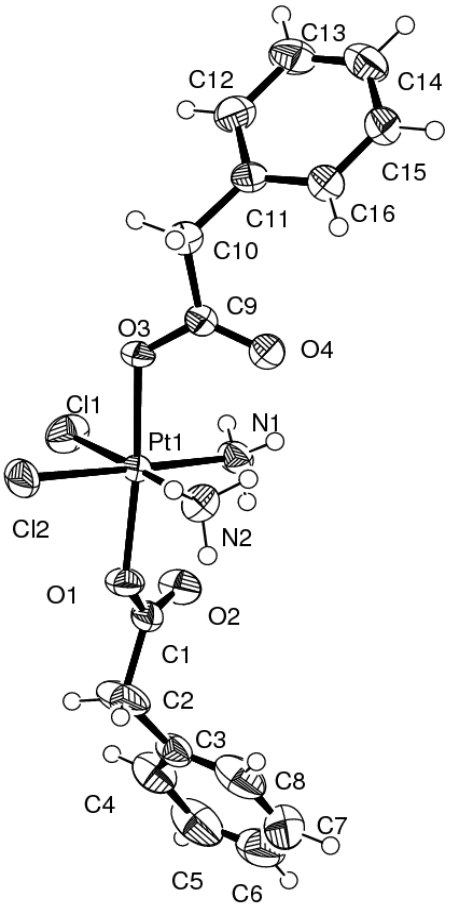
C13
C12
C14
C15
C11
C16
C10
C9
O3
O4
Cl1
Pt1
N1
Cl2
N2
O1
O2
C1
C2
C3
C8
C4
C7
C5
C6

Fig. 3.

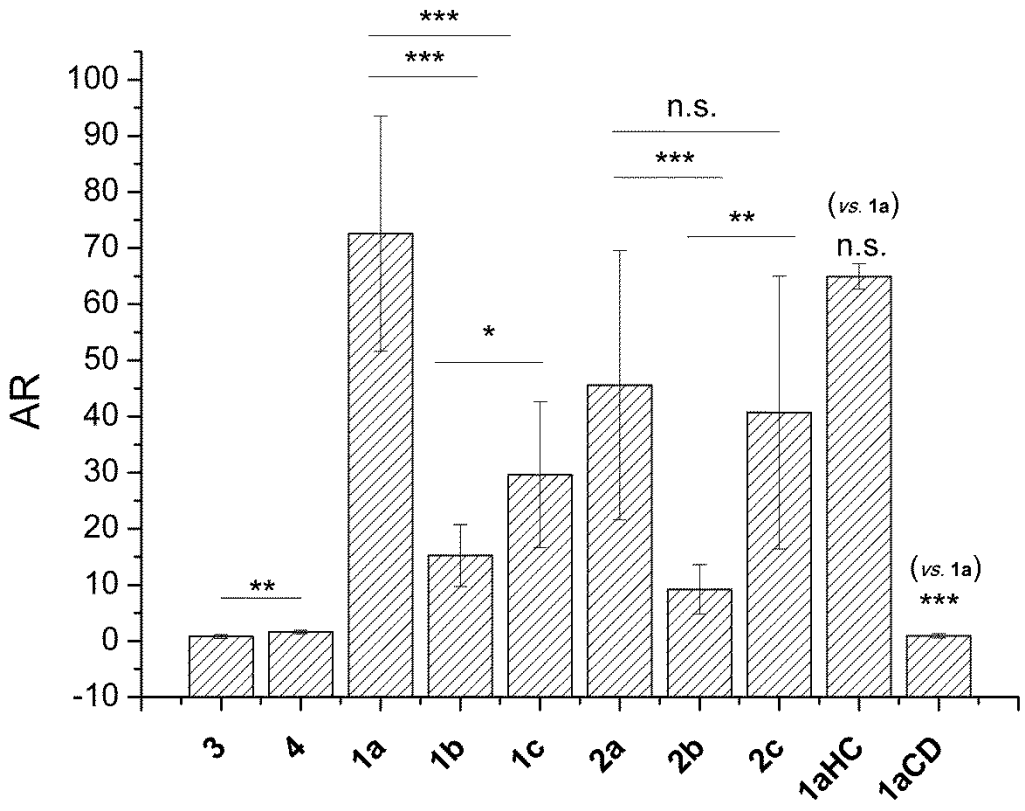
AR
100
90
80
70
60
50
40
30
20
10
0
-10
***
***
n.s.
***
**
(vs. 1a)
n.s.
*
**
(vs. 1a)
***
3
4
1a
1b
1c
2a
2b
2c
1aHC
1aCD

Fig. 4.

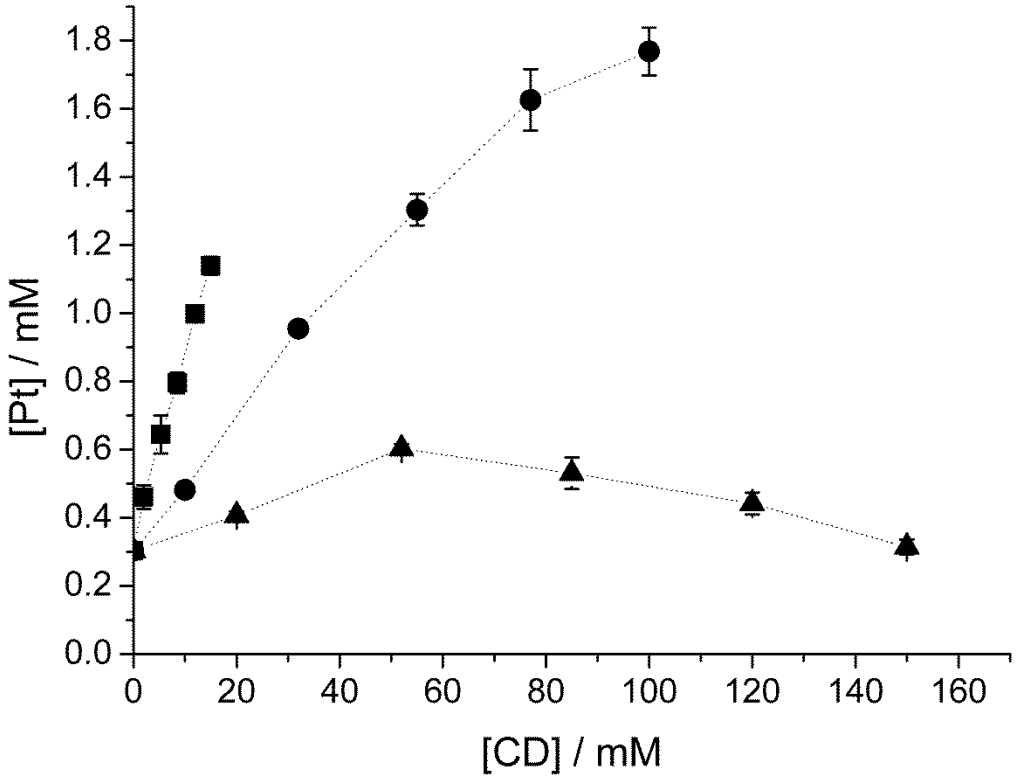

Fig. 5.

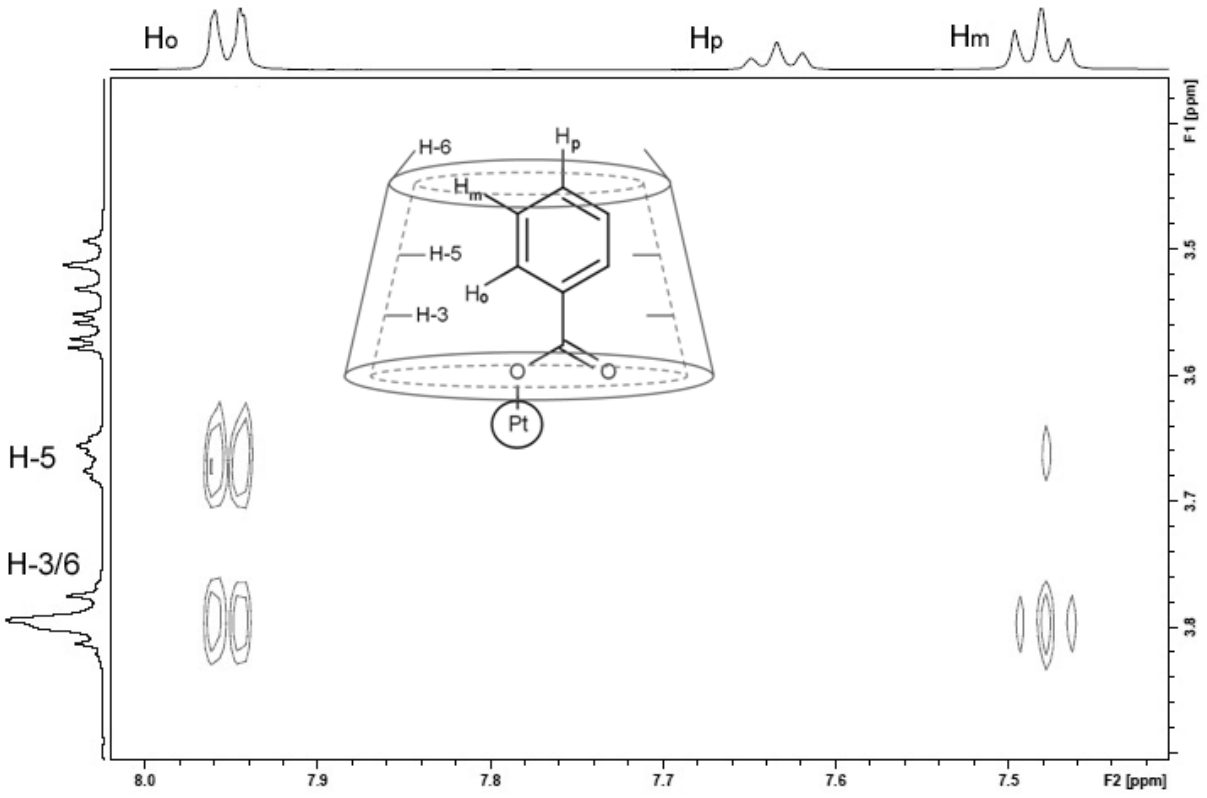
Ho
Hp
Hm
H-6
Hp
Hm
H-5
Ho
H-3
O
O
Pt
H-5
H-3/6
F1 [ppm]
3.5
3.6
3.7
3.8
8.0
7.9
7.8
7.7
7.6
7.5
F2 [ppm]

Fig. 6.

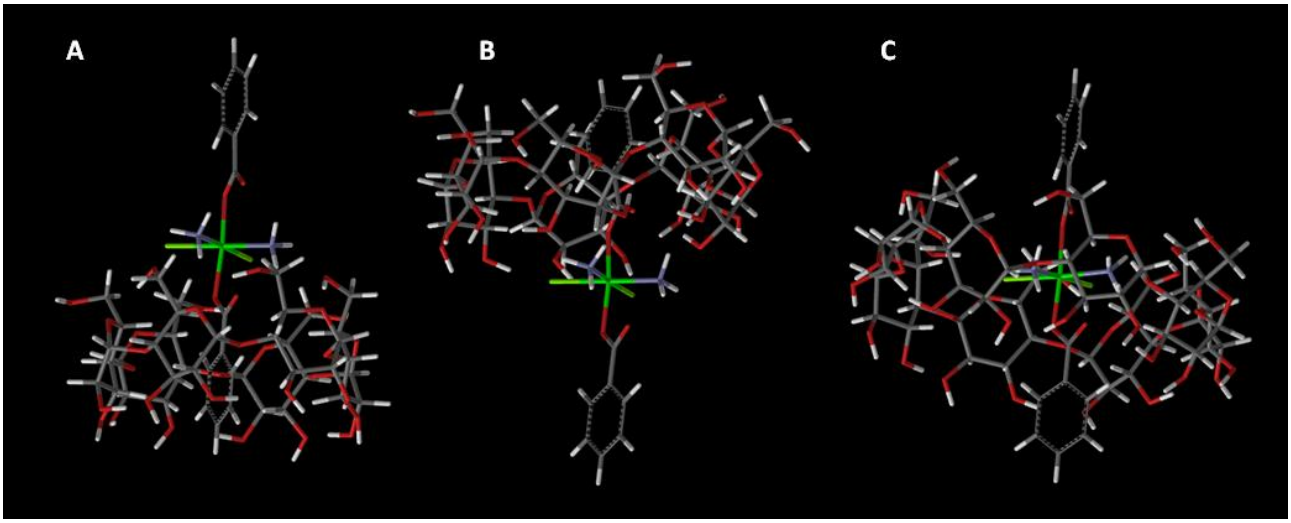
A
B
C

Fig. 7

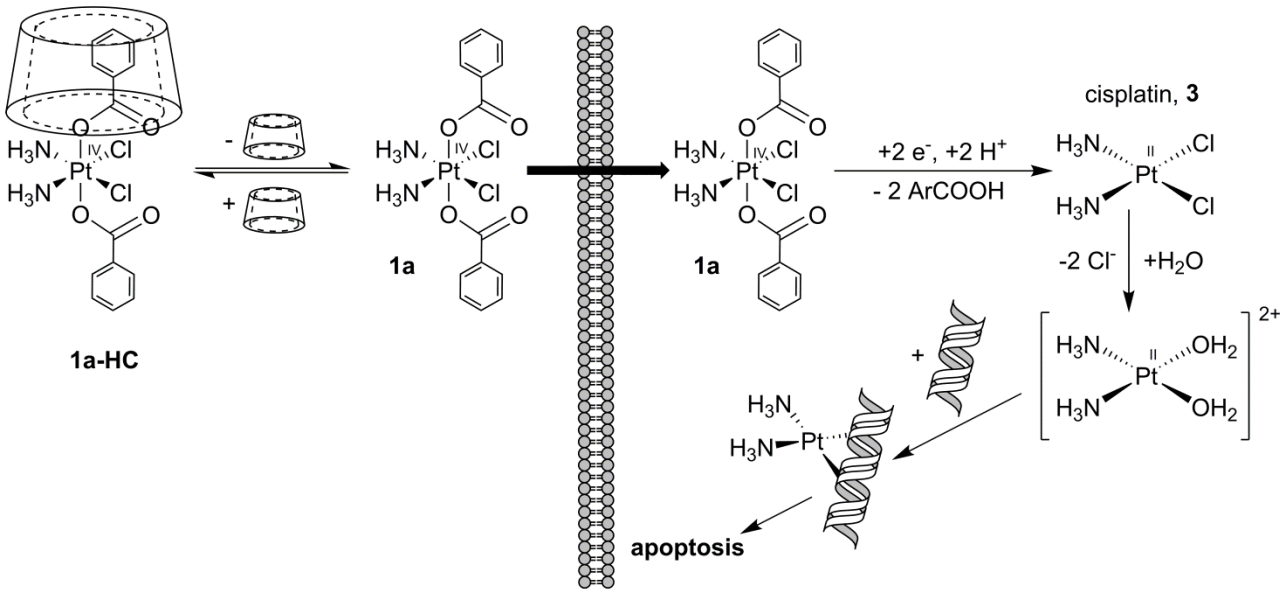

Fig. 8

Supplementary Info for online publication

Click here to download Supplementary Info for online publication: Osella_Pt(IV)_benzo_CD_Supp_Mat.docx

CIF File (if crystal structures are described)

Click here to download CIF File (if crystal structures are described): CCDC983761.cif

CIF Validation Report (if crystal structures are described)

Click here to download CIF Validation Report (if crystal structures are described): CCDC983761_checkcif.pdf